Endocrinology. First published ahead of print November 24, 2009 as doi:10.1210/en.2009-1163

Senescence Marker Protein-30/Gluconolactonase Deletion Worsens Glucose Tolerance through Impairment of Acute Insulin Secretion

Goji Hasegawa, Masahiro Yamasaki, Mayuko Kadono, Muhei Tanaka, Mai Asano, Takafumi Senmaru, Yoshitaka Kondo, Michiaki Fukui, Hiroshi Obayashi, Naoki Maruyama, Naoto Nakamura, and Akihito Ishigami

Department of Endocrinology and Metabolism (G.H., M.Y., M.K., M.T., M.A., T.S., M.F., N.N.), Kyoto Prefectural University of Medicine Graduate School of Medical Science, Kyoto 602-8556, Japan; Aging Regulation (Y.K., N.M.), Tokyo Metropolitan Institute of Gerontology, Tokyo 173-0015, Japan; Institute of Bio-Response Informatics (H.O.), Kyoto 612-8016, Japan; and Department of Biochemistry (A.I.), Faculty of Pharmaceutical Sciences, Toho University, Chiba 274-8510, Japan

Senescence marker protein-30 (SMP30) is an androgen-independent factor that decreases with age. We recently identified SMP30 as the lactone-hydrolyzing enzyme gluconolactonase (GNL), which is involved in vitamin C biosynthesis in animal species. To examine whether the age-related decrease in SMP30/GNL has effects on glucose homeostasis, we used SMP30/GNL knockout (KO) mice treated with L-ascorbic acid. In an ip glucose tolerance test at 15 wk of age, blood glucose levels in SMP30/GNL KO mice were significantly increased by 25% at 30 min after glucose administration compared with wild-type (WT) mice. Insulin levels in SMP30/GNL KO mice were significantly decreased by 37% at 30 min after glucose compared with WT mice. Interestingly, an insulin tolerance test showed a greater glucose-lowering effect in SMP30/GNL KO mice. High-fat diet feeding severely worsened glucose tolerance in both WT and SMP30/GNL KO mice. Morphometric analysis revealed no differences in the degree of high-fat diet-induced compensatory increase in β-cell mass and proliferation. In the static incubation study of islets, insulin secretion in response to 20 mM glucose or KCl was significantly decreased in SMP30/GNL KO mice. On the other hand, islet ATP content at 20 mM in SMP30/GNL KO mice was similar to that in WT mice. Collectively, these data indicate that impairment of the early phase of insulin secretion due to dysfunction of the distal portion of the secretion pathway underlies glucose intolerance in SMP30/GNL KO mice. Decreased SMP30/GNL may contribute to the worsening of glucose tolerance that occurs in normal aging. (***Endocrinology*** **151: 0000–0000, 2010)**

Senescence marker protein-30 (SMP30), a 34-kDa protein originally identified in rat liver, is a novel molecule whose expression decreases with age in a sex-independent manner (1, 2). SMP30 transcripts have been detected in multiple tissues, and its amino acid alignment reveals a highly conserved structure among humans, rats, and mice (2). We previously reported that SMP30 participates in Ca^{2+} efflux by activating the calmodulin-dependent Ca^{2+} pump in HepG2 cells and renal tubular cells, conferring on these cells a resistance to injury caused by high intracellular Ca^{2+} concentrations (3, 4). Recently, we identified SMP30 as glucolactonase (GNL), which is involved in L-ascorbic acid biosynthesis in mammals, although human beings are unable to synthesize vitamin C *in vivo* because there are many mutations in their gulonolactone oxidase gene, which catalyzes the conversion of L-gulono-γ-lactone to L-ascorbic acid (5).

To clarify the causal relationship between decreased SMP30/GNL and age-associated physiological changes, we created SMP30/GNL knockout (KO) mice (6). The

ISSN Print 0013-7227 ISSN Online 1945-7170
Printed in U.S.A.

doi: 10.1210/en.2009-1163 Received October 1, 2009. Accepted October 26, 2009.

Abbreviations: AUC, Area under the curve; BrdU, 5-bromo-2-deoxyuridine; GNL, gluconolactonase; HFD, high-fat diet; KO, knockout; NEFA, nonesterified fatty acid; SD, standard diet; SMP30, senescence marker protein-30; WT, wild-type.

livers of SMP30/GNL KO mice were highly susceptible to TNFα- and Fas-mediated apoptosis (6). In addition, their livers showed abnormal accumulation of triglycerides, cholesterol, and phospholipids (7). The lungs of SMP30/GNL KO mice developed alveolar air sac enlargement similar to the senile lung syndrome seen in some elderly people (8, 9). The deposition of lipofuscin, an aging marker, was observed in renal tubular epithelial cells in these mice (2). Furthermore, SMP30/GNL in the brain and lungs has been proposed to have protective effects against oxidative stress associated with aging (9, 10). Although the physiological function of SMP30/GNL is still not entirely clear, our studies using SMP30/GNL KO mice have revealed that a reduction in SMP30/GNL expression may account for the age-associated deterioration of cellular function and the enhanced susceptibility to harmful stimuli in aged tissue. Also, these mice displayed symptoms of scurvy when fed a vitamin C-deficient diet (5, 11–13).

The reduction of carbohydrate metabolism in the elderly is one of the hallmarks of the aging process, and substantial evidence shows that increasing age is associated with worsened glucose tolerance and type 2 diabetes (14, 15). However, the molecular abnormalities that occur in the elderly have not been fully elucidated. Because SMP30/GNL KO mice show phenotypic changes that mimic the premature aging process, we hypothesized that a reduction in SMP30/GNL expression could be linked to the worsening of glucose tolerance that occurs with normal aging. The purpose of this study was to examine the role of SMP30/GNL in glucose homeostasis using SMP30/GNL KO mice.

Materials and Methods

Animals

SMP30/GNL KO mice were generated as described earlier by gene targeting in the background strain C57BL/6 (6). All studies were performed on male mice using age-matched, wild-type (WT) male C57BL/6CrSlc mice (Shimizu Laboratory Supplies Co., Ltd., Kyoto, Japan) as controls. Mice were fed a high-fat diet (HFD 32; 507.6 kcal/100 g, fat kcal 56.7%; CLEA Japan, Tokyo, Japan) or a standard diet (SD; 346.8 kcal/100 g, fat kcal 10%, CLEA Japan) for 8 wk from 7 wk of age. As we have previously reported, SMP30/GNL KO mice cannot synthesize vitamin C *in vivo* because SMP30/GNL is a key enzyme involved in vitamin C biosynthesis (5). To avoid the effects of vitamin C deficiency, L-(+)-ascorbic acid (vitamin C, 1.5 g/liter) and 10 μM EDTA were added to the drinking water. The water was changed every 3 d until the experiment ended. Mice had free access to water and food and were maintained on a 12-h light, 12-h dark cycle with a controlled temperature. All experimental procedures were approved by the Committee for Animal Research, Kyoto Prefectural University of Medicine.

Analytic procedures and glucose and insulin tolerance tests

Blood glucose levels were measured using a glucometer (Gultest Ace; Sanwa Kagaku Kenkyusho Co., Ltd., Nagoya, Japan). To measure plasma lipids, blood was collected by cardiac puncture after an overnight fast just before the tissue collection. Plasma nonesterified fatty acid (NEFA), triglycerides, and total cholesterol were measured by the enzymatic method using an autoanalyzer. Intraperitoneal glucose (2 g/kg body weight) and insulin (0.75 U/kg body weight) tolerance tests were performed after 16- and 7-h fasts, respectively, and blood glucose was measured at the time indicated. For insulin release during glucose tolerance testing, the plasma component of blood collected at the 0- and 30-min time points was measured with an insulin enzyme immunoassay system, the Morinaga ultrasensitive mouse insulin assay kit (Morinaga Institute of Biological Science, Inc., Kanagawa, Japan).

Tissue collection and histological assessment of pancreatic islets

After an overnight fast, mice were killed by administration of an overdose of sodium aminobarbital. After blood collection by cardiac puncture, the lateral epididymal and inguinal sc adipose tissue depots were removed and weighed. A portion of the liver was used for measurement of total vitamin C content.

The whole pancreas was removed, cleared of fat and lymph nodes, weighed, fixed in 10% formalin solution, and embedded in paraffin. Pancreatic sections were prepared and stained with hematoxylin and eosin or an antibody against insulin using the Histofine mouse stain kit with a mouse antihuman insulin antibody (Nichirei Biosciences Inc., Tokyo, Japan). For morphometric analysis of β-cell mass, pancreatic sections 250 μm apart taken from three different levels of the pancreatic tissue block (five pancreases per experimental group) were examined. Nonoverlapping images were captured with a digital camera (Sony DXC-S500/OL; Sony, Tokyo, Japan). The β-cell area and the section area were analyzed using NIH Image J version 1.36b software. The β-cell mass was calculated by multiplying the pancreas weight by the percentage of β-cell area per pancreas.

To evaluate cell replication per islet, we performed labeling of proliferating cells with the DNA precursor analog 5-bromo-2-deoxyuridine (BrdU). Mice were injected ip with BrdU (1 mg/mouse; BD Biosciences, San Diego, CA) 12 h before being killed. After tissue processing as described above, immunostaining for BrdU was performed with a BrdU *in situ* detection kit (BD Biosciences) (16). All visible islets for each pancreatic section (three sections per animal) were analyzed to determine the total number of BrdU-positive cells and total islet count per section.

Measurement of pancreatic insulin content

Pancreatic insulin content was determined as previously described (17). Briefly, a portion of the pancreatic tail was homogenized in acidic ethanol (0.18 mol/liter HCl in 95% ethanol) and was extracted for 24 h at 4 C. The homogenate was centrifuged at 2000 × *g* for 15 min. Insulin levels in the supernatant were assayed as described above.

Measurement of total vitamin C levels in the liver

Livers were homogenized in 14 vol 5.4% metaphosphate, and then the homogenate was centrifuged at 21,000 × *g* for 15 min

at 4 C. Ascorbic acid in samples was treated with 0.1% dithiothreitol to reduce the dehydroascorbic acid to ascorbic acid and was analyzed by HPLC using an Atlantis dC18 5-μm column (4.6 × 150 mm; Nihon Waters, Tokyo, Japan) (11). The mobile phase was 50 mM phosphate buffer (pH 2.8), 0.2 g/liter EDTA, and 2% methanol at a flow rate of 1.3 ml/min, and electrical signals were recorded by using an electrochemical detector with a glassy carbon electrode at +0.6 V.

Static insulin secretion from isolated islets

Male SD-fed SMP30/GNL KO mice and C57BL/6CrSlc mice (14–15 wk of age) were used for islets isolation. Islets were isolated using collagenase (type V collagenase; Sigma Chemical Co., St. Louis, MO), digested in Hanks' buffer, followed by separation of islets from exocrine tissue in a Histopaque (Histopaque 1077; Sigma) gradient (18). Islets of similar size were hand picked under a stereomicroscope into groups (n = 5) of five islets in triplicate. The islets were preincubated for 60 min at 37 C in Krebs-Ringer bicarbonate HEPES buffer (equilibrated with 95% O_2 and 5% CO_2, pH 7.4) supplemented with 2 mg/ml BSA (fraction V; Sigma) and 2 mM glucose. After preincubation, five islets were incubated with 200 μl of the same buffer for 15 min. After samples from the buffer were removed for measurement of insulin, the islets were incubated in the presence of 20 mM glucose or 20 mM KCl plus 2 mM glucose for another 15 min. At the end of this period, the supernatant was collected. All samples were stored at −80 C until the insulin assay (Morinaga ultrasensitive mouse insulin assay kit).

ATP measurement from isolated islets

Cultured islets were preincubated at 37 C for 60 min in Krebs-Ringer bicarbonate HEPES buffer with 2 mM glucose, and then triplicate batches of 10 islets were incubated at 2 or 20 mM glucose for another 60 min. ATP was extracted from islets according to the methods described by Uchizono *et al.* (19). ATP levels were measured using the Enliten ATP assay system (Promega, Madison, WI) with a bioluminometer (GloMax 20/20n luminometer; Promega).

Statistical analysis

The data are expressed as means ± SE. Significance was determined by one-way ANOVA with Dunn's multiple comparisons *post hoc* or unpaired Student's *t* test where appropriate. A two-way ANOVA was used to compare the glucose and insulin levels on the same time point in ip glucose tolerance test. A value of $P < 0.05$ was considered to be significant.

Results

Energy intake, body weight, and adipose tissue

The mean energy intakes of the WT mice fed a SD, WT mice fed a HFD, SMP30/GNL KO mice fed an SD, and SMP30/GNL KO mice fed an HFD throughout the study were 9.1 ± 0.1, 13.1 ± 0.2, 8.5 ± 0.1, and 11.8 ± 0.2 kcal/d, respectively. All four groups of mice gained weight; however, the increase in body weight in the HFD-fed WT and HFD-fed SMP30/GNL KO mice was significantly higher than that in SD-fed WT and SD-fed SMP30/GNL KO mice (Fig. 1). The weight gain in the SD-fed WT, SD-fed SMP30/GNL KO, HFD-fed WT, and HFD-fed SMP30/GNL KO mice after 8 wk on the diets was 8.4 ± 0.4, 8.2 ± 0.4, 16.5 ± 0.7, and 14.7 ± 0.7 g/mouse, respectively. The HFD-fed WT mice gained 51% more weight than the SD-fed WT mice, and HFD-fed SMP30/GNL KO mice gained 56% more weight than the SD-fed SMP30/GNL KO mice.

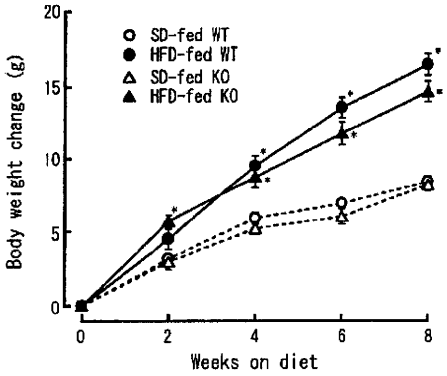

FIG. 1. Body weight changes of SD-fed and HFD-fed WT and SMP30/GNL KO mice. Experimental diets were started at 7 wk of age and continued for 8 wk (until 15 wk of age). *, $P < 0.01$ *vs.* SD-fed WT and SMP30/GNL KO mice. Data are means ± SE (n = 10 per group).

Epididymal fat pads from HFD-fed WT and HFD-fed SMP30/GNL KO mice after 8 wk on the diet were significantly heavier than fat pads from the SD-fed WT and SD-fed SMP30/GNL KO mice (Table 1). The ratio of epididymal fat mass to sc fat mass in HFD-fed WT and HFD-fed SMP30/GNL KO mice was also larger than in SD-fed WT and SD-fed SMP30/GNL KO mice, although the differences were not significant.

Total vitamin C levels in the liver

To examine the vitamin C status of the SMP30/GNL KO mice, we determined the total vitamin C content in the liver after 8 wk on the diets. The total vitamin C levels in the liver from SD-fed and HFD-fed WT mice and SD-fed and HFD-fed SMP30/GNL KO mice were 188.2 ± 12.3, 176.6 ± 8.9, 160.2 ± 7.4, and 150.4 ± 6.9 μg/g tissue, respectively. There were no significant differences among the four groups.

Blood glucose and plasma lipid levels

Fasting glucose levels of HFD-fed WT and HFD-fed SMP30/GNL KO mice after 8 wk on HFD were significantly increased in both groups compared with SD-fed WT and SD-fed SMP30/GNL KO mice (Table 1).

After 8 wk on HFD, HFD-fed WT and HFD-fed SMP30/GNL KO mice showed significant increases in total plasma cholesterol levels from 61–67% compared with SD-fed WT and SD-fed SMP30/GNL KO mice; however, there was no significant difference in plasma total

TABLE 1. Fasting glucose, plasma lipids, and adipose tissue weight after 8 wk on diet (15 wk of age)

	SD		HFD	
	WT	SMP30/GNL KO	WT	SMP30/GNL KO
Fasting glucose (mg/dl)	109.5 ± 3.7	101.6 ± 5.0	129.6 ± 6.4[a]	138.3 ± 6.7[a]
NEFA (mEq/liter)	1487.0 ± 79.0	1439.2 ± 56.6	927.9 ± 40.6[a]	882.1 ± 39.8[a]
Triglycerides (mg/dl)	106.4 ± 3.2	93.8 ± 4.5	74.6 ± 5.4[a]	69.8 ± 4.8[a]
Total cholesterol (mg/dl)	117.3 ± 2.7	108.1 ± 2.4	191.5 ± 10.2[b]	161.5 ± 6.6[a]
Epididymal fat (mg/g BW)	12.6 ± 1.5	9.0 ± 1.0	23.5 ± 1.9[a]	18.8 ± 2.1[a]
sc fat (mg/g BW)	5.9 ± 1.1	3.3 ± 0.5[b]	7.5 ± 0.5	5.5 ± 0.4
Epi/Sub	2.5 ± 0.4	2.9 ± 0.3	3.3 ± 0.4	3.4 ± 0.3

Data are means ± SE from 10 mice. BW, Body weight; Epi/Sub, ratio of epididymal fat mass to sc fat mass.

[a] $P < 0.05$ *vs.* SD-fed WT and SMP30/GNL KO mice.

[b] $P < 0.05$ *vs.* the other three groups.

cholesterol levels between SD-fed WT and SD-fed SMP30/GNL KO mice (Table 1). Compared with the mice fed SD, mice fed HFD had lower triglyceride and NEFA levels. However, there was no difference in triglyceride and NEFA levels between WT and SMP30/GNL KO mice. This paradoxical decrease in triglycerides and NEFAs is consistent with a previous report showing that the C57BL/6 strain has a unique metabolic response to HFD (20). These data indicate that deficiency of SMP30 has no influence on lipid profile either in SD-fed or in HFD-fed animal.

Intraperitoneal glucose tolerance test

Blood glucose levels at 30 min after glucose administration were 25% higher in SD-fed SMP30/GNL KO mice than in SD-fed WT mice ($P < 0.05$, Fig. 2A). And blood glucose levels at 30, 60, and 120 min after glucose administration were significantly higher in HFD-fed WT and HFD-fed SMP30/GNL KO mice than in SD-fed WT and SD-fed SMP30/GNL KO mice. Moreover, the blood glucose levels of HFD-fed SMP30/GNL KO mice at 60 and 120 min after glucose administration were significantly higher than those of HFD-fed WT mice. The areas under the curve (AUC, 0–120 min) in SD-fed and HFD-fed WT mice and SD-fed and HFD-fed SMP30/GNL KO mice were 417.1 ± 18.3, 721.2 ± 41.7, 496.1 ± 36.2, and 900.2 ± 40.6 mg · h/dl, respectively (ANOVA, $P < 0.0001$). It is noteworthy that the AUC did not differ between SD-fed WT and SD-fed SMP30/GNL KO mice ($P = 0.128$). This result indicates that the significantly high blood glucose levels appeared restrictively at 30 min after glucose administration in SD-fed SMP30/GNL KO mice.

There were no significant differences in fasting insulin levels between SD-fed WT and SD-fed SMP30/GNL KO mice (Fig. 2B). However, insulin levels of SD-fed SMP30/GNL KO mice at 30 min after glucose were 37% lower than those of SD-fed WT mice ($P < 0.05$). HFD feeding increased fasting insulin levels in both WT and SMP30/GNL KO mice; however, those of SMP30/GNL KO mice were 39% lower than those of WT mice. Similarly, insulin levels at 30 min after glucose were 27% lower in HFD-fed SMP30/GNL KO mice compared with those of HFD-fed WT mice. The AUC (0–30 min) in SD-fed and HFD-fed WT mice and SD-fed and HFD-fed SMP30/GNL KO mice were 1.09 ± 0.08, 1.86 ± 0.19, 0.71 ± 0.11, and 1.19 ± 0.12 ng · 30 min/ml, respectively (ANOVA, $P < 0.0001$). The AUC in SD-fed SMP30/GNL KO mice was lower than that in SD-fed WT mice, although the difference was not statistically significant ($P = 0.052$).

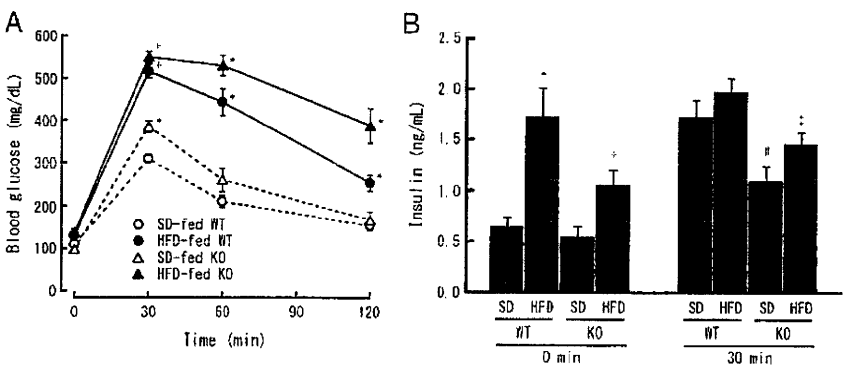

FIG. 2. Impaired glucose tolerance in WT and SMP30/GNL KO mice after 8 wk of SD or HFD feeding. A, Intraperitoneal glucose tolerance test; B, insulin levels at baseline and at 30 min after glucose. *, $P < 0.05$ *vs.* the other three groups; †, $P < 0.05$ *vs.* SD-fed WT and SMP30/GNL KO mice; #, $P < 0.05$ *vs.* SD-fed and HFD-fed WT mice; ‡, $P < 0.05$ *vs.* HFD-fed WT mice. Data are means ± SE (n = 7 per group).

Insulin tolerance test

We next assessed insulin sensitivity using an insulin tolerance test. Blood glucose levels in SD-fed SMP30/GNL KO mice were significantly reduced to 49 and 51% of the levels of SD-fed WT mice after 30 and 60 min, respectively, indicating high peripheral insulin sensitivity (Fig. 3). HFD-fed SMP30/GNL KO mice showed similar insulin tolerance to that of SD-fed WT mice.

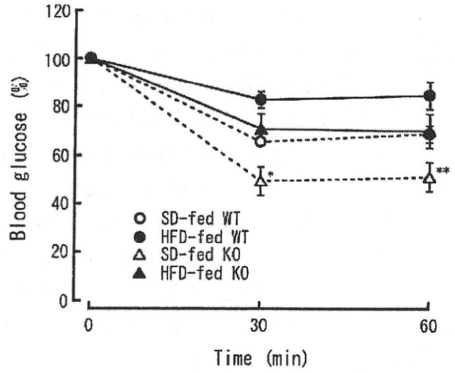

FIG. 3. Intraperitoneal insulin tolerance test after 8 wk of SD or HFD feeding. Data are expressed as percentage of basal (0 min) glucose levels. *, $P < 0.05$ *vs.* HFD-fed WT and SMP30/GNL KO mice; **, $P < 0.05$ *vs.* the other three groups. Data are means ± SE (n = 7 per group).

β-Cell mass and proliferation

The pancreas weight per body weight was significantly lower in SD-fed SMP30/GNL KO mice than in SD-fed WT mice (Table 2). Eight weeks of HFD feeding increased the pancreas weight of SMP30/GNL KO mice to the same level as SD-fed and HFD-fed WT mice. Morphometric analyses of β-cell mass, as assessed by immunohistochemical analysis, revealed no differences between SMP30/GNL KO mice and WT mice (Table 2). HFD feeding significantly increased β-cell mass in both WT and SMP30/GNL KO mice to similar levels. Similarly, there were no significant differences in pancreatic insulin content in response to HFD feeding between WT and SMP30/GNL KO mice (Table 2).

Hematoxylin and eosin staining revealed no differences in islet morphology among the four groups. The proliferation of islet cells, which was determined by the frequency of BrdU-positive cells per islet, in both HFD-fed WT and SMP30/GNL KO mice was significantly higher than in animals fed SD (Fig. 4 and Table 2). In addition, there was no difference in islet proliferation between SMP30/GNL KO and WT mice. This finding demonstrates that the proliferation of β-cells to compensate for increased insulin demand is not impaired in SMP30/GNL KO mice. However, insulin levels of SD-fed SMP30/GNL KO mice at 30 min after glucose were 37% lower than those of SD-fed WT mice.

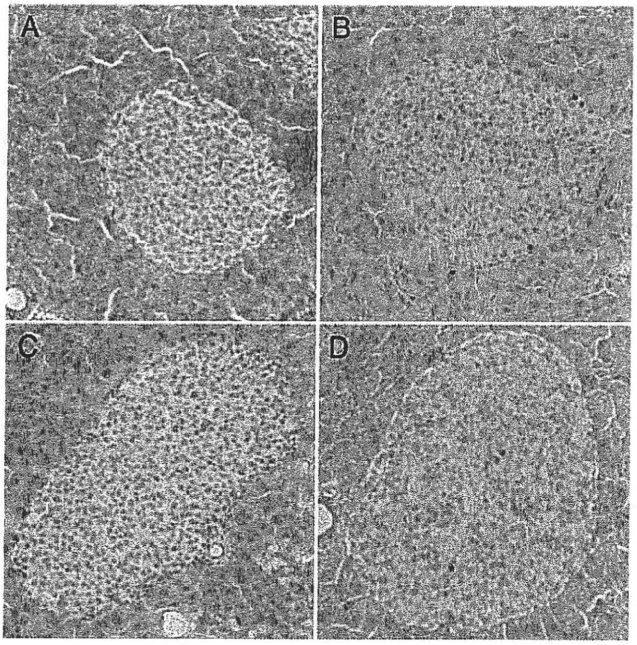

FIG. 4. Immunohistochemical staining of BrdU in pancreas sections. Mice were injected with BrdU 12 h before being killed. BrdU-positive cells (*brown*) were observed in the islets of both WT (B) and SMP30/GNL KO mice (D) on the HFD. A and C, WT (A) and SMP30/GNL KO mice (C) on the SD. Magnification, ×100.

Insulin secretion and ATP measurements from isolated islets

To confirm β-cell dysfunction in SMP30/GNL KO mice, we measured insulin secretion in response to glucose and KCl from the isolated islets. The basal insulin secretion in SD-fed SMP30/GNL KO and WT mice were 89.3 ± 9.8 and 93.3 ± 10.4 pg/islet · 15 min (n = 10), respectively. There were no significant differences between the two. Similar to *in vivo* results, insulin secretion of SD-fed SMP30/GNL KO mice in 20 mM glucose for 15 min was significantly reduced compared with those of SD-fed WT mice ($P < 0.05$, Fig. 5A). Insulin secretory response to 20

TABLE 2. Morphometric analysis and insulin contents of pancreases after 8 wk of SD or HFD feeding

	Pancreas weight (mg/g body weight), n = 10	Pancreatic insulin content (μg/g pancreas), n = 10	β-Cell mass (mg), n = 5	BrdU index (%), n = 5
SD				
WT	5.4 ± 0.4	42.1 ± 3.9	1.21 ± 0.21	4.4 ± 2.8
SMP30/GNL KO	4.1 ± 0.2[a]	40.4 ± 4.6	1.14 ± 0.13	6.9 ± 3.5
HFD				
WT	5.4 ± 0.2	56.7 ± 4.9[b]	3.28 ± 0.85[b]	37.3 ± 11.7[b]
SMP30/GNL KO	5.6 ± 0.4	53.1 ± 4.1[b]	2.83 ± 0.41[b]	47.3 ± 10.6[b]

BrdU index: total BrdU positive islet cells/total islet counts per section.

[a] $P < 0.05$ *vs.* the other three groups.

[b] $P < 0.05$ *vs.* SD-fed WT and SMP30/GNL KO mice.

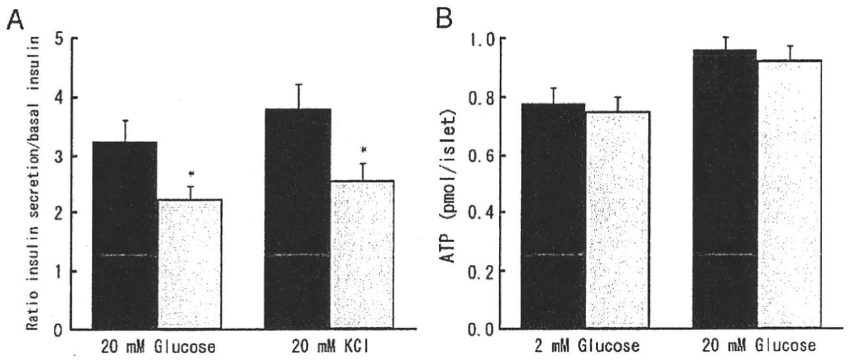

FIG. 5. Insulin secretion and ATP content in islets isolated from WT (*black bars*) and SD-fed SMP30/GNL KO mice (*gray bars*) (14–15 wk of age). A, Static islet incubation for 15 min in 20 mM glucose or 20 mM KCl. The data are expressed as ratio of 15 min to basal insulin (picograms per islet per 15min). *, $P < 0.05$ *vs.* WT mice. Data are means ± SE (n = 5 per group). B, ATP content at 2 and 20 mM glucose. There were no significant differences in ATP content at 2 or 20 mM glucose between WT and SMP30/GNL KO mice. Data are means ± SE (n = 5 per group).

mM KCl was also reduced significantly in SMP30/GNL KO mice ($P < 0.05$, Fig. 5A).

Islet ATP content was significantly elevated at 20 mM glucose compared with 2 mM glucose in SD-fed SMP30/GNL KO and WT mice. However, there were no significant differences in ATP content at 2 or 20 mM glucose between the two (Fig. 5B).

Discussion

This is the first report documenting impaired glucose tolerance in SMP30/GNL-deficient mice and provides new insight into the possible role of SMP30/GNL in glucose homeostasis. Our *in vitro* data using isolated islets confirmed that deletion of SMP30/GNL was responsible for the reduced insulin secretory response to glucose. The present study differs from previous studies using SMP30/GNL KO mice, in that the mice were maintained with a sufficient supply of vitamin C. This eliminated the confounding secondary effects of vitamin C on glucose homeostasis and made this experimental model more relevant to human disease.

SMP30/GNL KO mice at 15 wk of age demonstrated mild glucose intolerance compared with WT mice. They also showed an impairment in acute insulin secretion after glucose administration and better peripheral insulin sensitivity as assessed by an insulin tolerance test. These data suggest that an impairment of the early phase of insulin secretion underlies the glucose intolerance seen in SMP30/GNL KO mice. In HFD-fed WT mice as well as in SMP30/GNL KO mice, HFD feeding increased fat mass and worsened glucose tolerance. However, this impairment of glucose tolerance was more pronounced in SMP30/GNL KO mice. This difference likely reflects SMP30/GNL KO mice's intrinsic reduction in insulin secretion capacity, as shown by their impaired acute insulin secretion after a glucose load and similar insulin resistance to WT mice when fed an HFD. It has been reported that vitamin C treatment has no effect on insulin secretion in diabetic C57BL/KsJ-db/db mice or nondiabetic control mice (21). Thus, the differential vitamin C status seen in this study is unlikely to be the cause of the impairment of insulin secretion.

It is interesting that SMP30/GNL KO mice had the higher peripheral insulin sensitivity. The better insulin sensitivity might partially compensate for the decreased insulin secretion and made the moderate impairment of glucose tolerance. Although the present data could not refer to its mechanism, the lower epididymal and sc fat mass in SMP30/GNL KO mice may help account for the result. Now, we can just assume that absence of SMP30/GNL in insulin-sensitive tissues, including liver, kidney, fat, and muscle, may directly affect insulin signaling pathway or secondarily affect insulin action through metabolic pathways. Also, an increased insulin clearance from the liver is another possibility. It is well known that increased insulin resistance is a major factor involved in impaired glucose tolerance in the elderly. So we would say that SMP30/GNL KO mice is not an appropriate animal model of impaired glucose tolerance in normal aging.

The static incubation study of islets demonstrated the reduced insulin secretory response to glucose and KCl in SMP30/GNL-deficient mice. KCl depolarizes the β-cell plasma membrane, which initiates a series of events such as Ca^{2+} influx, mobilization of Ca^{2+} from intracellular stores, and insulin exocytosis. On the other hand, glucose-stimulated insulin secretion from the β-cell occurs after generation of ATP from metabolism of glucose through glycolysis and the Krebs cycle. The intracellular rise in ATP/ADP ratio leads to closure of the K_{ATP} channels, Ca^{2+} influx, and subsequent activation of insulin secretion. The reduced insulin secretory response to KCl, together with the preservation of ATP production, suggests that events in the distal portion of the insulin secretion pathway are impaired in SMP30/GNL-deficient mice. The mechanism underlying β-cell dysfunction in SMP30/GNL KO mice has not been fully explored. However, previous reports have proposed the possibility of dysregulation of Ca^{2+} homeostasis. SMP30/GNL maintains Ca^{2+} homeostasis by enhancing plasma membrane Ca^{2+}-pumping activity (3, 4). Therefore, taken together with the present results of *in vitro* islet study, a deficiency of SMP30/GNL

may induce dysregulation of Ca^{2+} homeostasis, resulting in impairment of the increase in Ca^{2+} influx resulting from a high glucose concentration and of Ca^{2+}-dependent signaling pathways, which are involved in the mechanisms of insulin secretion. Additional studies, such as intracellular calcium levels in β-cells may allow for a more precise localization of these abnormalities.

It has been well documented that HFD feeding induces compensatory β-cell hyperplasia in response to insulin resistance in mice (22, 23). In the present study, too, HFD feeding caused insulin resistance in both WT and SMP30/GNL KO mice, but there were no differences in the degree of compensatory increase in β-cell mass and proliferation between WT and SMP30/GNL KO mice. These findings suggest that SMP30/GNL deficiency causes β-cell dysfunction without impairment of the mechanism responsible for islet hyperplasia.

Both decreased insulin secretion and increased insulin resistance are two major factors involved in impaired glucose tolerance in the elderly. Increased adiposity and decreased physical activity contribute to insulin resistance in the elderly (15). Recent reports indicate that the age-associated decline in muscle mitochondrial function is a mechanism for insulin resistance (24). On the other hand, the molecular mechanism for the development of age-dependent β-cell defects is still unknown. Aging could be associated with a loss of β-cell mass or impaired β-cell function or a combination of these two factors (25–27). The present results suggest the possibility that a reduction in SMP30/GNL with age contributes to the age-related impairment of β-cell function. If this is the case, SMP30/GNL could be a novel molecule that is involved not only in the impaired insulin secretion that occurs with normal aging but also in the pathogenesis of type 2 diabetes.

In summary, SMP30/GNL KO mice have modestly impaired glucose tolerance with an impairment of acute insulin secretion due to dysfunction of the distal portion of the secretion pathway. The increase in β-cell mass and proliferation to compensate for insulin resistance is equivalent to that of WT mice. The present results suggest that reduction in SMP30/GNL could be a factor that contributes to the worsening of glucose tolerance with normal aging and that this mechanism may provide new insights into the age-associated pathophysiology of β-cell function.

Acknowledgments

We thank Fumie Takenaka, Hiroko Kawamura, and Sayoko Horibe for their secretarial assistance. Vitamin C powder was kindly provided by DSM Nutrition Japan (Tokyo, Japan).

Address all correspondence and requests for reprints to: Goji Hasegawa, M.D., Department of Endocrinology and Metabolism, Kyoto Prefectural University of Medicine Graduate School of Medical Science, 465 Kajii-cho, Hirokoji, Kawaramachi-dori, Kamikyo-ku, Kyoto 602-8566, Japan. E-mail: goji@koto.kpu-m.ac.jp.

This work was supported by Grants-in-Aid for Scientific Research (20591066 to G.H. and 18590355 to A.I.) from the Japan Society for the Promotion of Science.

Disclosure Summary: The authors have nothing to disclose.

References

1. **Fujita T, Uchida K, Maruyama N** 1992 Purification of senescence marker protein-30 (SMP30) and its androgen-independent decrease with age in the rat liver. Biochim Biophys Acta 1116:122–128
2. **Ishigami A, Maruyama N** 2007 Significance of SMP30 in gerontology. Geriatr Gerontol Int 7:316–325
3. **Fujita T, Inoue H, Kitamura T, Sato N, Shimosawa T, Maruyama N** 1998 Senescence marker protein-30 (SMP30) rescues cell death by enhancing plasma membrane Ca^{2+}-pumping activity in Hep G2 cells. Biochem Biophys Res Commun 250:374–380
4. **Inoue H, Fujita T, Kitamura T, Shimosawa T, Nagasawa R, Inoue R, Maruyama N, Nagasawa T** 1999 Senescence marker protein-30 (SMP30) enhances the calcium efflux from renal tubular epithelial cells. Clin Exp Nephr 3:261–267
5. **Kondo Y, Inai Y, Sato Y, Handa S, Kubo S, Shimokado K, Goto S, Nishikimi M, Maruyama N, Ishigami A** 2006 Senescence marker protein 30 functions as gluconolactonase in L-ascorbic acid biosynthesis, and its knockout mice are prone to scurvy. Proc Natl Acad Sci USA 103:5723–5728
6. **Ishigami A, Fujita T, Handa S, Shirasawa T, Koseki H, Kitamura T, Enomoto N, Sato N, Shimosawa T, Maruyama N** 2002 Senescence marker protein-30 knockout mouse liver is highly susceptible to tumor necrosis factor-α- and Fas-mediated apoptosis. Am J Pathol 161:1273–1281
7. **Ishigami A, Kondo Y, Nanba R, Ohsawa T, Handa S, Kubo S, Akita M, Maruyama N** 2004 SMP30 deficiency in mice causes an accumulation of neutral lipids and phospholipids in the liver and shortens the life span. Biochem Biophys Res Commun 315:575–580
8. **Mori T, Ishigami A, Seyama K, Onai R, Kubo S, Shimizu K, Maruyama N, Fukuchi Y** 2004 Senescence marker protein-30 knockout mouse as a novel murine model of senile lung. Pathol Int 54:167–173
9. **Sato T, Seyama K, Sato Y, Mori H, Souma S, Akiyoshi T, Kodama Y, Mori T, Goto S, Takahashi K, Fukuchi Y, Maruyama N, Ishigami A** 2006 Senescence marker protein-30 protects mice lungs from oxidative stress, aging, and smoking. Am J Respir Crit Care Med 174:530–537
10. **Son TG, Zou Y, Jung KJ, Yu BP, Ishigami A, Maruyama N, Lee J** 2006 SMP30 deficiency causes increased oxidative stress in brain. Mech Ageing Dev 127:451–457
11. **Furusawa H, Sato Y, Tanaka Y, Inai Y, Amano A, Iwama M, Kondo Y, Handa S, Murata A, Nishikimi M, Goto S, Maruyama N, Takahashi R, Ishigami A** 2008 Vitamin C is not essential for carnitine biosynthesis in vivo: verification in vitamin C-depleted senescence marker protein-30/gluconolactonase knockout mice. Biol Pharm Bull 31:1673–1679
12. **Kondo Y, Sasaki T, Sato Y, Amano A, Aizawa S, Iwama M, Handa S, Shimada N, Fukuda M, Akita M, Lee J, Jeong KS, Maruyama N, Ishigami A** 2008 Vitamin C depletion increases superoxide generation in brains of SMP30/GNL knockout mice. Biochem Biophys Res Commun 377:291–296
13. **Sato Y, Kajiyama S, Amano A, Kondo Y, Sasaki T, Handa S, Takahashi R, Fukui M, Hasegawa G, Nakamura N, Fujinawa H, Mori T, Ohta M, Obayashi H, Maruyama N, Ishigami A** 2008 Hydrogen-rich pure water prevents superoxide formation in brain

slices of vitamin C-depleted SMP30/GNL knockout mice. Biochem Biophys Res Commun 375:346–350
14. **Chang AM, Halter JB** 2003 Aging and insulin secretion. Am J Physiol Endocrinol Metab 284:E7–E12
15. **Scheen AJ** 2005 Diabetes mellitus in the elderly: insulin resistance and/or impaired insulin secretion? Diabetes Metab 31(Spec No 2): 5S27–25S34
16. **Robertson H, Wheeler J, Morley AR** 1990 In vivo bromodeoxyuridine incorporation in normal mouse kidney: immunohistochemical detection and measurement of labelling indices. Histochem J 22: 209–214
17. **Hasegawa G, Mori H, Sawada M, Takagi S, Shigeta H, Kitagawa Y, Nakano K, Kanatsuna T, Kondo M** 1990 Dietary treatment ameliorates overt diabetes and decreased insulin secretion to glucose induced by overeating in impaired glucose tolerant mice. Horm Metab Res 22:408–412
18. **Lacy PE, Kostianovsky M** 1967 Method of the isolation of intact islets of Langerhans from the rat pancreas. Diabetes 16:35–39
19. **Uchizono Y, Iwase M, Nakamura U, Sasaki N, Goto D, Iida M** 2004 Tacrolimus impairment of insulin secretion in isolated rats islets occurs at multiple distal sites in stimulus-secretion coupling. Endocrinology 145:2264–2272
20. **Colombo C, Haluzik M, Cutson JJ, Dietz KR, Marcus-Samuels B, Vinson C, Gavrilova O, Reitman ML** 2003 Opposite effects of background genotype on muscle and liver insulin sensitivity of lipoatrophic mice. Role of triglyceride clearance. J Biol Chem 278:3992–3999
21. **Kaneto H, Kajimoto Y, Miyagawa J, Matsuoka T, Fujitani Y, Umayahara Y, Hanafusa T, Matsuzawa Y, Yamasaki Y, Hori M** 1999 Beneficial effects of antioxidants in diabetes: possible protection of pancreatic β-cells against glucose toxicity. Diabetes 48:2398–2406
22. **Sone H, Kagawa Y** 2005 Pancreatic β-cell senescence contributes to the pathogenesis of type 2 diabetes in high-fat diet-induced diabetic mice. Diabetologia 48:58–67
23. **Terauchi Y, Takamoto I, Kubota N, Matsui J, Suzuki R, Komeda K, Hara A, Toyoda Y, Miwa I, Aizawa S, Tsutsumi S, Tsubamoto Y, Hashimoto S, Eto K, Nakamura A, Noda M, Tobe K, Aburatani H, Nagai R, Kadowaki T** 2007 Glucokinase and IRS-2 are required for compensatory β-cell hyperplasia in response to high-fat diet-induced insulin resistance. J Clin Invest 117:246–257
24. **Petersen KF, Befroy D, Dufour S, Dziura J, Ariyan C, Rothman DL, DiPietro L, Cline GW, Shulman GI** 2003 Mitochondrial dysfunction in the elderly: possible role in insulin resistance. Science 300:1140–1142
25. **Chang AM, Smith MJ, Galecki AT, Bloem CJ, Halter JB** 2006 Impaired β-cell function in human aging: response to nicotinic acid-induced insulin resistance. J Clin Endocrinol Metab 91:3303–3309
26. **Maedler K, Schumann DM, Schulthess F, Oberholzer J, Bosco D, Berney T, Donath MY** 2006 Aging correlates with decreased β-cell proliferative capacity and enhanced sensitivity to apoptosis: a potential role for Fas and pancreatic duodenal homeobox-1. Diabetes 55:2455–2462
27. **Szoke E, Shrayyef MZ, Messing S, Woerle HJ, van Haeften TW, Meyer C, Mitrakou A, Pimenta W, Gerich JE** 2008 Effect of aging on glucose homeostasis: accelerated deterioration of β-cell function in individuals with impaired glucose tolerance. Diabetes Care 31: 539–543

Journal of Neuroscience Research

Journal of Neuroscience Research 88:798–806 (2010)

Developmental and Age-Related Changes of Peptidylarginine Deiminase 2 in the Mouse Brain

Nobuko Shimada,[1] Setsuko Handa,[1] Yoshiaki Uchida,[2] Mitsugu Fukuda,[1] Naoki Maruyama,[1] Hiroaki Asaga,[3] Eun-Kyoung Choi,[4] Jaewon Lee,[5] and Akihito Ishigami[1,6]*

[1]Aging Regulation, Tokyo Metropolitan Institute of Gerontology, Tokyo, Japan
[2]Fujirebio, Inc., Tokyo, Japan
[3]Biological Science Laboratory, Meiji University, Tokyo, Japan
[4]Ilsong Institute of Life Science, Hallym University, Gyeonggi-do, Republic of Korea
[5]Department of Pharmacy, College of Pharmacy, Longevity Life Science and Technology Institute, Pusan National University, Busan, Republic of Korea
[6]Department of Biochemistry, Faculty of Pharmaceutical Sciences, Toho University, Chiba, Japan

Peptidylarginine deiminases (PADs) are a group of posttranslational modification enzymes that citrullinate (deiminate) protein arginine residues in a Ca^{2+}-dependent manner. Enzymatic citrullination abolishes positive charges of native protein molecules, inevitably causing significant alterations in their structure and functions. Among the five isoforms of PADs, PAD2 and PAD4 are proved occupants of the central nervous system (CNS), and especially PAD2 is a main PAD enzyme expressed in the CNS. We previously reported that abnormal protein citrullination by PAD2 has been closely associated with the pathogenesis of neurodegenerative disorders such as Alzheimer's disease and prion disease. Protein citrullination in these patients is thought to play a role during the initiation and/or progression of disease. However, the contribution of changes in PAD2 levels, and consequent citrullination, during developmental and aging processes remained unclear. Therefore, we used quantitative real-time RT-PCR, Western blot analysis, and immunohistochemical methods to measure PAD2 expression and localization in the brain during those processes. PAD2 mRNA expression was detected in the brains of mice as early as embryonic day 15, and its expression in cerebral cortex, hippocampus, and cerebellum increased significantly as the animals aged from 3 to 30 months old. No citrullinated proteins were detected during that period. Moreover, we found here, for the first time, that PAD2 localized specifically in the neuronal cells of the cerebral cortex and Purkinje cells of the cerebellum. These findings indicate that, despite PAD2's normally inactive status, it becomes active and citrullinates cellular proteins, but only when the intracellular Ca^{2+} balance is upset during neurodegenerative changes.

Key words: cerebellum; citrullination; neurodegenerative disorder; PAD2; Purkinje cells

Because concentrations of peptidylarginine deiminases (PADs; EC 3.5.3.15) become altered during developmental and aging processes and have been linked to abnormal accumulations of citrullinated proteins in degenerative diseases of the brain, we sought to establish in detail the levels and impact of PADs in neonatal and aging mice. PADs are posttranslational modification enzymes that citrullinate (deiminate) protein arginine residues in a calcium ion-dependent manner, yielding citrulline residues (Watanabe et al., 1988; Vossenaar et al., 2003). Enzymatic citrullination abolishes positive charges of native protein molecules, thereby altering their structure and functions over time (Tarcsa et al., 1996). Although the five isoforms of PADs (i.e., types 1, 2, 3, 4/5, and 6) reside in multiple mammalian tissues (Watanabe et al., 1988; Vossenaar et al., 2003), their tissue-specific expression differs according to analysis by reverse transcriptase-polymerase chain reaction (RT-PCR; Ishigami et al., 2001). However, all these isoforms display nearly identical amino acid sequences (Ishigami et al., 2002). Among them, PAD2 and PAD4 occupy the central nervous system (CNS), and especially PAD2 is a main PAD enzyme expressed in the CNS.

These isoforms are present in myelin sheath, and hypercitrullination of myelin basic protein (MBP) resulted in loss of myelin sheath integrity in multiple sclerosis (MS)

The first two authors contributed equally to this work.

Contract grant sponsor: Ministry of Education, Science, and Culture, Japan (to N.S., A.I.).

*Correspondence to: Akihito Ishigami, PhD, Department of Biochemistry, Faculty of Pharmaceutical Sciences, Toho University, Miyama 2-2-1, Funabashi, Chiba 274-8510, Japan. E-mail: ishigami@phar.toho-u.ac.jp

Received 10 April 2009; Revised 20 July 2009; Accepted 24 July 2009

Published online 14 October 2009 in Wiley InterScience (www.interscience.wiley.com). DOI: 10.1002/jnr.22255

patients (Moscarello et al., 1994; Musse et al., 2008; Wood et al., 2008). Moreover, PAD4, the nuclear isoform of this family of enzymes, is involved in histone citrullination in the MS brain (Mastronardi et al., 2006). Immunocytochemical studies have localized PAD2 in glial cells, especially astrocytes (Asaga and Ishigami, 2000, 2001), microglial cells (Asaga et al., 2002), and oligodendrocytes (Akiyama et al., 1999). Additionally, PAD2 expression was later detected in cultured Schwann cells (Keilhoff et al., 2008). However, although the presence of PAD2 in glial cells should have imbued them with citrullinated proteins, such proteins were rarely identified in those cells examined with our sensitive detection method (Senshu et al., 1992). Therefore, we assumed that PAD2 is normally inactive (Asaga and Ishigami, 2000, 2001; Asaga et al., 2002). However, under abnormal conditions, glial fibrillary acidic protein (GFAP) was highly susceptible to the attack of PAD2 in excised rat brains deliberately left at room temperature (Asaga and Senshu, 1993). Under hypoxic conditions (Asaga and Ishigami, 2000) and during kainic acid-evoked neurodegeneration (Asaga and Ishigami, 2001; Asaga et al., 2002), PAD2 became activated in regions undergoing neurodegeneration and functioned to citrullinate various cerebral proteins, indicating the involvement of protein citrullination in neurodegenerative processes. These findings provided an important clue; that is, PAD2 normally remains inactive but becomes active and citrullinates cellular proteins only when the intracellular calcium balance is upset during neurodegenerative changes. In fact, our previous report indicated that citrullinated proteins including GFAP, vimentin, and myelin basic protein (MBP) accumulated to an abnormal extent in the Alzheimer's disease (AD)-afflicted hippocampus and that the expression of PAD2 increased during related neurodegenerative changes (Ishigami et al., 2005). We subsequently described increases of the citrullinated proteins GFAP, MBP, enolases, and aldolases in the brains of mice infected with scrapie as a model of prion disease along with the increased expression and activity of PAD2, suggesting that accumulated citrullinated proteins and abnormal activation of PAD2 may play a role in the pathogenesis of prion diseases. Moreover, in patients with MS, citrullinated MBP was increased to 45% of total MBP compared with much smaller amounts in healthy adults (Moscarello et al., 1994) and was later regarded as a pathological mechanism of MS (Moscarello et al., 2007).

Because PAD2 activation and accumulation of citrullinated proteins in the brain are increasingly associated with the progression of neurodegenerative disorders such as AD, prion disease, and MS, it is very important to clarify the expression and localization of PAD2 in the brain during the developmental and aging process. For comparison of PAD2 expression and characteristic localization, we used microtubule-associated protein 2 (MAP2) and neurofilament 3 (Nef3) as neuronal cell markers and GFAP as a marker of astrocyte in this study. After applying quantitative real-time RT-PCR, Western blot analysis, and immunohistochemical methods, we found that PAD2 mRNA expression levels increased significantly in the cerebral cortex, hippocampus, and cerebellum during aging. Moreover, for the first time, PAD2 was identified in neuronal cells of the cerebral cortex and Purkinje cells of the cerebellum.

MATERIALS AND METHODS

Animals

Male C57BL/6 mice 3, 6, 12, 24, or 30 months of age were obtained from the Animal Facility at Tokyo Metropolitan Institute of Gerontology, and pregnant female mice were obtained from Japan SLC (Shizuoka, Japan). Mice at the embryonic days 15, 16, 17, and 18; postnatal days 1, 2, 3, 7, and 30; and ages 3, 6, 12, 24, and 30 months were used in this study. Throughout the experiments, animals were maintained on 12-hr light/dark cycles in a controlled environment. All experimental procedures using laboratory animals were approved by the Animal Care and Use Committee of Tokyo Metropolitan Institute of Gerontology.

Brain Sample Preparation

Mice were anesthetized and systemically perfused with phosphate-buffered saline to wash out blood cells. Their brains were quickly excised and divided into cerebral cortex, hippocampus, and cerebellum. Brain sections were homogenized in 10 mM Tris-HCl (pH 7.6) containing 1 mM phenylmethylsulfonyl fluoride and centrifuged at 21,000*g* for 10 min at 4°C. For Western blot analysis, the supernatants were boiled for 5 min with a lysis buffer containing 0.125 M Tris-HCl (pH 6.8), 4% SDS, 20% glycerol, 10% 2-mercaptoethanol, and 0.2% bromophenol blue in a ratio of 1:1 and kept at −80°C until use. The protein concentration was determined by BCA protein assay (Pierce Biotechnology, Rockford, IL) using bovine serum albumin as a standard. To prepare total RNA, the brain sections were immediately frozen in liquid nitrogen and stored at −80°C until use. For immunohistochemical staining, brain tissues were immersed in 10% formalin (Wako Pure Chemical, Osaka, Japan) and left standing for 48 hr. Each fixed brain was cut in half laterally, then embedded in paraffin, and finally cut serially into 6-μm-thick cryosections. Human brain samples were obtained from the Brain Bank for Aging Research (BBAR) organized by the Tokyo Metropolitan Geriatric Hospital and Tokyo Metropolitan Institute of Gerontology (TMIG). Human studies were approved by the Ethics Committees of the TMIG.

PAD2 Monoclonal Antibody

The entire coding sequence of human PAD2 (hPAD2; GenBank AB030176) was amplified by PCR using primers, pENTR-hPAD2 forward primer 5′-CACCATGCTGCGCGAGCGGACCGTGCGGCTG-3′ and pENTR-hPAD2 reverse primer 5′-CCGGAATTCGCGGCCGCTCTGGGCGTGTGAGGGAGGGTCTGGAG-3′. The PCR products were subcloned in pENTR/D-TOPO vector (Invitrogen, Carlsbad, CA). To produce N-terminal 6× his-tagged hPAD2-recombinant protein, hPAD2 cDNA was subcloned to pDEST17 vector (Invitrogen) and transformed with the BL21-AI strain of *Escherichia coli*. The transformants were grown overnight, then treated for 4 hr with 0.2% L-arabinose at 37°C. The bacteria were then disrupted by sonication, and the recombinant proteins were purified by using Ni-NTA

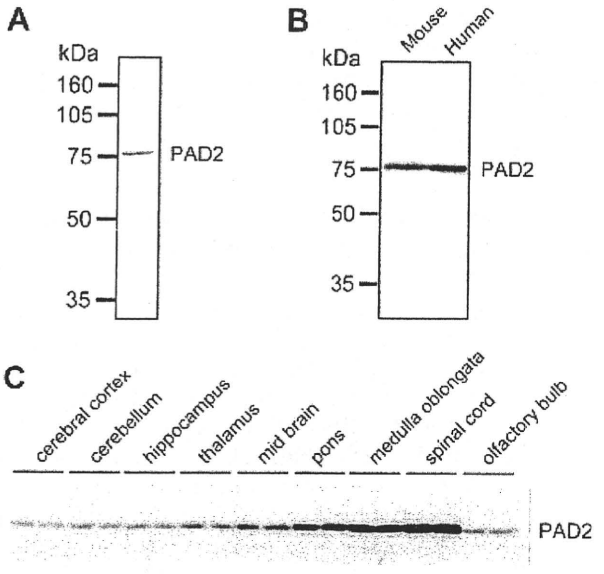

Fig. 1. Characterization of the anti-hPAD2 monoclonal antibody hPAD2-2110 and distribution of PAD2 protein in the CNS. **A:** Purified recombinant hPAD2 protein was separated on 10% SDS-PAGE, followed by Coomassie brilliant blue staining. **B:** Mouse and human brain samples were prepared as described in Materials and Methods. Ten micrograms of extracted proteins were separated on 10% SDS-PAGE and then electrotransferred onto a PVDF membrane. PAD2 was detected by using anti-hPAD2 monoclonal antibody. **C:** Under the stereoscopic microscope, each brain from 3-month-old mice was divided into nine parts: the cerebral cortex, cerebellum, hippocampus, thalamus, midbrain, pons, medulla oblongata, spinal cord, and olfactory bulb. From each part, 10 μg of extracted proteins was separated on 10% SDS-PAGE. PAD2 was detected by using anti-hPAD2 monoclonal antibody. Analyses were performed in duplicate with samples from two individual mice.

agarose beads (Qiagen, Valencia, CA). The identity of recombinant hPAD2 proteins was verified by sodium dodecyl sulfate (SDS)- polyacrylamide gel electrophoresis (PAGE), followed by Coomassie brilliant blue staining (see Fig. 1A).

Purified recombinant hPAD2 (50 μg) in complete Freund's adjuvant was injected into BALB/c mice, which were then given a booster injection of the same antigen in incomplete Freund's adjuvant. Three days after the last injection, spleen cells were fused with mouse P3U1 myeloma cells by using polyethylene glycol, and fused cells were cultured with HAT medium (Invitrogen). The specificities of hPAD2 monoclonal antibody-producing cells, hPAD2-264, hPAD2-2110, hPAD2-2111, hPAD2-2147, hPAD2-2153, hPAD2-2167 clones, were determined by enzyme-linked immunosorbent assays and Western blot analysis. Only the anti-hPAD2 monoclonal antibody hPAD2-2110 was purified from ascites by protein G Sepharose 4 Fast Flow columns (GE Healthcare, Piscataway, NJ). Anti-hPAD2 monoclonal antibody hPAD2-2110 reacted with both human and mouse PAD2 in the brain as confirmed by Western blot analysis (Fig. 1B).

Western Blot Analysis

Equal amounts of protein (10 μg/lane) were separated by SDS-PAGE on vertical slab 10% polyacrylamide gels (1 mm × 9 cm) by the method of Laemmli (1970). Proteins were then electrophoretically transferred from polyacrylamide gels onto a membrane of poylvinylidene difluoride (PVDF; Millipore, Billerica, MA) by the method of Towbin et al. (1979). The membrane was then incubated successively with anti-hPAD2 monoclonal antibody (hPAD2-2110; 1:1,000) and horseradish peroxidase-labeled goat anti-mouse IgG (Bio-Rad, Hercules, CA). Chemiluminescence signals were detected with a LAS-3000 imaging system (Fujifilm, Tokyo, Japan) using ECL Western Blotting Detection Reagents (GE Healthcare UK Ltd. Amersham, Little Chalfont, Buckinghamshire, United Kingdom). Signal intensity was analyzed by using Multi Gauge software (Fujifilm).

RT-PCR

Total RNA was extracted by using Isogen (Wako Pure Chemical, Osaka, Japan). Brain samples were homogenized with a Teflon-pestle homogenizer in Isogen, and total RNA was extracted according to the supplier's instructions. The final RNA pellet was dissolved in diethyl pyrocarbonate-treated H_2O, and the RNA concentration was determined and confirmed to be free from protein contamination by measuring absorbance at 260 and 280 nm. Five micrograms of total RNA from each sample was treated with Turbo DNase I (Ambion, Austin, TX) to eliminate any trace of genomic DNA. RT-PCR was performed with a Takara mRNA Selective PCR Kit (Takara, Kyoto, Japan) according to the supplier's instructions. Reverse transcription was performed with antisense oligonucleotide primers. Mouse PAD2 primers were designed in the 3′ noncording region of the cDNA after checking the absence of homology with any other PAD sequences by using the Blast program. The sense and antisense primers used were, for mouse PAD2, 5′-CTGCGG TCTCTGGGTCCTTCCTGTA-3′ and 5′-GACCAGGC-GAGAGAACAGAAATAGC-3′ (expected size 665 bp; Watanabe and Senshu, 1989); for mouse GFAP, 5′-CTGGAGG TGGAGAGGGACAACTT-3′ and 5′-CCGCATCTCCA-CAGTCTTTACCA-3′ (expected size 840 bp; Balcarek and Cowan, 1985); for mouse MAP2, 5′-GTGAACAAGA-GAAGGAAGCCCAACA-3′ and 5′-GGACCTGCTTGGG-GACTGTGTGATG-3′ (expected size 956 bp; Lewis et al., 1988); and, for mouse glyceraldehyde-3-phosphate dehydrogenase (GAPDH), 5′-GTGAAGGTCGGTGTGAACGGAT-3′ and 5′-GCCGCCTGCTTCACCACCTTCTT-3′ (expected size 788 bp; Tso et al., 1985). PCR conditions were 30 sec at 94°C, followed by 25, 30, or 40 cycles at 94°C for 30 sec, 60°C for 30 sec, and 72°C for 1 min, and a terminal extension period (72°C, 5 min). PCR products were visualized by gel electrophoresis in 1.2% agarose with ethidium bromide staining. To confirm their identity, PCR products were subcloned and sequenced.

Quantitative Real-Time PCR Analysis

A final preparation of 1.8 μg for each total RNA was subjected to two-step quantitative real-time PCR. In the first step, reverse transcription reaction was carried out with a random primer and SuperScript II (Invitrogen) in the presence of RNase inhibitor. For the second step, synthesized cDNA was

applied to the inventoried TaqMan gene expression assay by using the real-time PCR equipment (Applied Biosystems 7300 Real Time PCR System; Applied Biosystems, Foster City, CA). For quantitative analysis, a standard curve method was designed using a common standard prepared by mixing an aliquot of all samples from the experiment, and the standard was diluted serially to compute the threshold cycle covering the range between 18 and 35. The samples were also diluted properly for each of the target genes and GAPDH to be measured on the linear range of the semilogarithmic standard curve. All assays were performed under the standard curve correlation factor above 0.990. Values of unknown samples were corrected for dilution factor and normalized to the GAPDH level assumed as a constant. The expression of PAD2, GFAP, and Nef3 was analyzed, and the results are shown as percentage value; i.e., the level at postnatal day 30 and hippocampus at 3-months-old was considered as 100%. All assays were performed in duplicate.

Immunohistochemical Staining

After removal of paraffin, the brain sections were heated by microwave in 0.1 M citrate buffer (pH 7.0), followed by inactivation of endogenous peroxidase during incubation with 1% hydrogen peroxide in methanol. The primary antibodies used were mouse monoclonal PAD2 antibody (hPAD2-2110, 1:1,000), rabbit polyclonal GFAP antibody (1:1,000; Cosmo Bio, Tokyo, Japan), and mouse monoclonal MAP2 antibody (1:1,000; Chemicon, Temecula, CA). PAD2, GFAP, and MAP2 were detected by indirect immunoperoxidase staining using corresponding Histofine Simple Stain MAX-PO kits (Nichirei Biosciences, Tokyo, Japan) and 3,3′-diaminobenzidine (DAB) as a chromogenic substrate. After DAB staining, nuclei were counterstained with Myer's hematoxylin.

For double staining of PAD2 and calbindin-D-28K (calbindin), rabbit anticalbindin antibody (Thermo Fisher Scientific, Fremont, CA) was reacted first, and the alkaline phosphatase-conjugated anti-rabbit IgG (Histofine; Nichirei Biosciences) was reacted to stain with a Red Alkaline Phosphate Substrate Kit I. Second, anti-PAD2 monoclonal antibody (hPAD2-2110) was reacted, then horseradish peroxidase-conjugated anti-mouse IgG was reacted to stain with DAB.

Statistical Analysis

Results are expressed as mean ± SEM. The probability of statistical differences between experimental groups was determined by Bonferroni's multiple-comparisons test subsequent to one-way ANOVA. A statistical difference was considered significant at $P < 0.05$.

RESULTS

Distribution of PAD2 Protein in the CNS

We searched for PAD2 protein throughout the CNS by examining the cerebral cortex, cerebellum, hippocampus, thalamus, midbrain, pons, medulla oblongata, spinal cord, and olfactory bulb of 3-month-old mice. Western blot analysis revealed PAD2 protein in all these regions (Fig. 1C). Specifically, we calculated a ratio of PAD2 protein in the cerebellum, hippocampus, thalamus, midbrain, pons, medulla oblongata, spinal cord, and olfactory bulb compared with the amount of PAD2 protein in the cerebral cortex as 1.3-fold, 1.4-fold, 1.7-fold, 2.3-fold, 3.8-fold, 5.6-fold, 9.9-fold, and 1.6-fold, respectively.

Developmental Change of PAD2 mRNA Expression Level in the Whole Brain

To assess our assumption that PAD2 mRNA expression levels undergo developmental changes, we examined whole brains of mice from embryonic day 15 to postnatal day 30 by both RT-PCR and quantitative real-time PCR. Small amounts of PAD2 mRNA were detected at 15 days of embryonic life and increased slightly until birth (Fig. 2A,B). After birth, the PAD2 mRNA level was constant until the third postnatal day and then significantly increased 2.5-fold at day 7 and 9.9-fold at day 30 compared with value at postnatal day 3 (Fig. 2B). Moreover, the PAD2 mRNA level at 30 days after birth was a statistically significant 3.9-fold higher than that at the seventh postnatal day. Similarly, amounts of PAD2 protein in the whole brain were small at embryonic day 16, held constant until the third postnatal day, then significantly increased to 5.9-fold at 7 days and to 17-fold at 30 days after birth compared with the amount of PAD2 protein at the third postnatal day (Western blot analysis; Fig. 3).

GFAP as a marker of astrocyte mRNA was detected at 16 days of embryonic life and increased until 3 postnatal days, then continued to increase until reaching a significant increment at the seventh and again at the thirtieth postnatal days (Fig. 2A,C). The GFAP mRNA level at 7 days and 30 days after birth also rose significantly to 3.4-fold and 2.4-fold higher levels than that at 3 days after birth (Fig. 2C). On the other hand, mRNAs for MAP2 and Nef3, the neuronal cell markers, were detectable in 15-day-old embryos and increased slightly until birth (Fig. 2A,D). The Nef3 mRNA level at 30 days of postnatal was a significant 1.3-fold higher than that at postnatal day 7 (Fig. 2D).

Age-Related Change of PAD2 mRNA Expression Level

The age-related changes of PAD2, GFAP, and Nef3 mRNA in the cerebral cortex, cerebellum, and hippocampus of 3-month-old to 30-month-old mice were analyzed by quantitative real-time PCR. PAD2 mRNA expression was detected in the cerebral cortex, cerebellum, and hippocampus, but the cerebral cortex contained significantly less PAD2 mRNA than was found in the cerebellum and hippocampus regardless of the animals' ages (Fig. 4A). Moreover, PAD2 mRNA levels at all three sites gradually increased during aging. PAD2 mRNA levels in the cerebral cortex, cerebellum, and hippocampus at 30 months were about 1.6-fold, 1.5-fold, and 1.6-fold higher, respectively, than in 3-month-old animals.

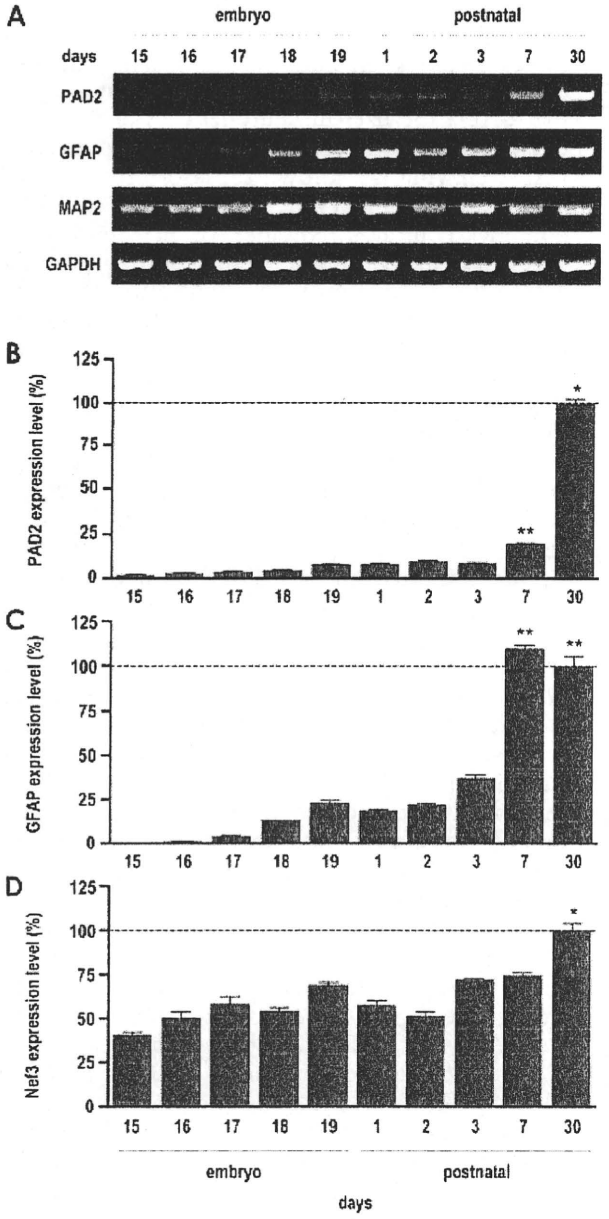

Fig. 2. Developmental changes of PAD2, GFAP, MAP2, and Nef3 mRNA expression levels in the whole brains of mice. **A:** RT-PCR was carried out with 1 μg of total RNA and specific oligonucleotide primer of PAD2, GFAP, MAP2, and GAPDH as described in Materials and Methods. An aliquot of each PCR product was electrophoresed in 1.2% agarose gel and stained with ethidium bromide for detection under UV light. **B–D:** Quantitative real-time PCR analysis was carried out with TaqMan primers and probes specific to PAD2 (B), GFAP (C), and Nef3 (D). As the endogenous control, GAPDH was quantified simultaneously and used to normalize each raw data point. Data from quantitative real-time PCR are shown as the percentage of each value, with postnatal day 30 taken as 100%, and represent mean ± SEM of five animals. $*P < 0.05$ compared with 15–19 days of embryonic life and 1–3 or 7 days after birth. $**P < 0.05$ compared with 15–19 days of embryonic life and 1–3 days after birth.

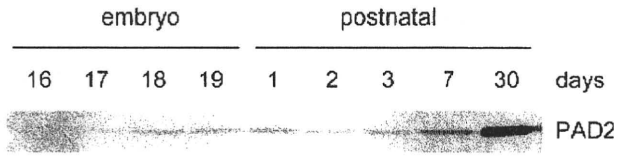

Fig. 3. Western blot analysis of PAD2 protein in the whole brain during development from embryonic day 16 to postnatal day 30. Ten micrograms of protein extracted from the whole brain was separated on 10% SDS-PAGE and then electrotransferred onto the PVDF membrane. PAD2 was detected by using anti-hPAD2 monoclonal antibody, hPAD2-2110.

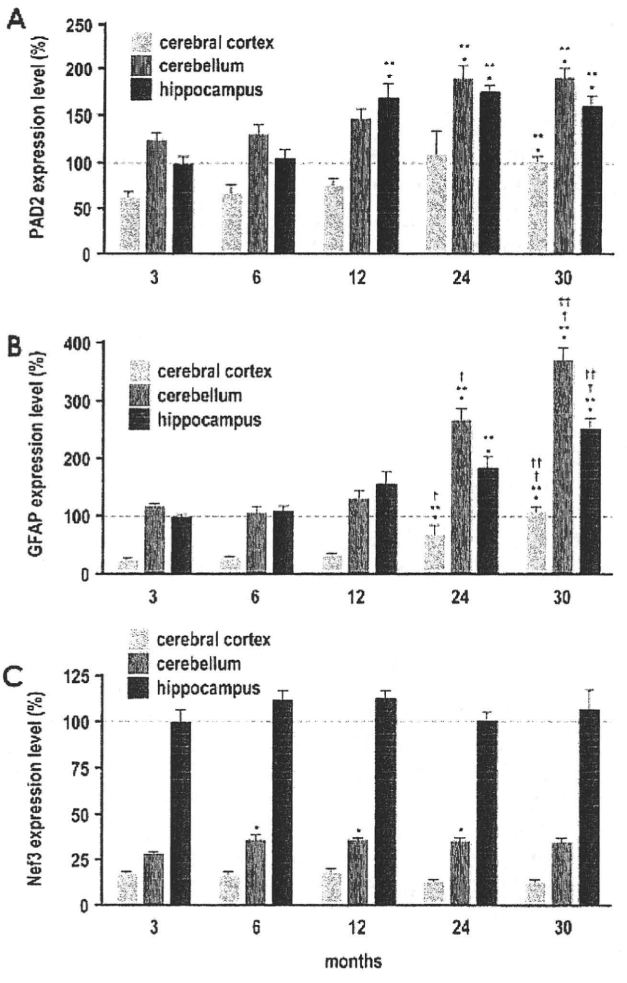

Fig. 4. Age-dependent changes of PAD2, GFAP, and Nef3 mRNA expression in the brain. Total RNA from the cerebral cortex, cerebellum, and hippocampus of 3-, 6-, 12-, 24-, and 30-month-old mice was prepared. Quantitative real-time PCR analysis of PAD2 (**A**), GFAP (**B**), and Nef3 (**C**) was carried out as described in Materials and Methods. As the endogenous control, GAPDH was quantified simultaneously to normalize each raw data. Data are expressed in percentages, with values in the hippocampus of 3-month-old mice taken as 100%, and represent a mean ± SEM of five animals. $*P < 0.05$ compared with 3-month-old mice. $**P < 0.05$ compared with 6-month-old mice. $^{\dagger}P < 0.05$ compared with 12-month-old mice. $\dagger\dagger P < 0.05$ compared with 24-month-old mice.

Similarly, GFAP mRNA expression in the cerebral cortex, cerebellum, and hippocampus gradually increased during aging, although the GFAP mRNA content in the cerebral cortex was significantly lower than that in the cerebellum and hippocampus at all ages (Fig. 4B). GFAP expression in the cerebral cortex, cerebellum, and hippocampus at 30 months was about 4.2-fold, 3.1-fold, and 2.5-fold higher than in 3 month-old-mice, respectively. On the other hand, Nef3 mRNA expression was detected in the cerebral cortex, cerebellum, and hippocampus and was abundantly expressed in the hippocampus of mice at all ages tested. Moreover, Nef3 mRNA expression levels in all regions did not change during aging (Fig. 4C).

Immunohistochemical Localization of PAD2 in the Cerebral Cortex, Cerebellum, and Hippocampus

To establish firmly that PAD2-positive cells are present in the cerebral cortex, hippocampus, and cerebellum of 3-month-old mice, we performed immunohistochemical staining of serial sections by using PAD2-, GFAP-, and MAP2-specific antibody (Fig. 5). In the cerebral cortex and hippocampus, PAD2-positive signals were detected in neuronal cell bodies that costained with MAP2 (Fig. 5G,H,M,N) but not in dendrites. Not only was MAP2 staining positive in both the neuronal cell bodies and the dendrites, but the cerebral cortex, hippocampus, and cerebellum were also MAP2-positive (Fig 5M–O). However, GFAP-positive cells, which are considered to be reactive astrocytes, were PAD2 negative in the cerebral cortex, hippocampus, and cerebellum (Fig. 5G–L).

In the cerebellum, PAD2-positive staining was present on morphologically characteristic Purkinje-like cells along dense granule cell layers that were not positive for either MAP2 or GAFP (Fig. 5I,L,O). To confirm that these were actually Purkinje cells, we performed double immunostaining with PAD2 and calbindin, a known marker of Purkinje cells and limited to localization in those cells (Servais et al., 2005; Whitney et al., 2008; Fig. 6). Calbindin staining was evident as a light magenta coloration on the alkaline phosphate substrate (Fig. 6A). These Purkinje cells appeared as huge, round cell bodies located between the bottom of the molecule layer and surface of the granule cell layer of cerebellar tissue. PAD2 was stained brown by the DAB used as a chromogenic substrate (Fig. 6B). Double immunostaining allowed detection of both calbindin- and PAD2-positive cells in the same Purkinje cells from the cerebellum (Fig. 6C), thus ensuring the existence of PAD2 in clearly identified Purkinje cells of the cerebellum. Additionally, the characteristic localization of PAD2, GFAP, and MAP2 in the cerebral cortex, hippocampus, and cerebellum did not change during aging from 3 months to 30 months (data not shown).

DISCUSSION

We report here, for the first time, that PAD2 mRNA expression increases significantly in the cerebral cortex, hippocampus, and cerebellum during aging and that PAD2 localizes in neuronal cells of the cerebral cortex and Purkinje cells of cerebellum. Activation of the PAD2 enzyme is a known cause of protein citrullination (Watanabe et al., 1988; Vossenaar et al., 2003). The potential clinical importance of the findings presented here lies in the close association previously found between abnormal protein citrullination in the CNS and the neurodegenerative disorders AD (Ishigami et al., 2005), MS (Moscarello et al., 2007) and prion disease (Jang et al., 2008). However, until now, changes of PAD2 expression levels have not been linked with the aging process.

In this study, PAD2 mRNA expression was detected in the brains of mice after 15 days of embryonic development, and GFAP mRNA expression first became evident just 1 day later (Fig. 1B,C). Previous reports indicated that PAD2 appeared mainly in glial cells, especially astrocytes (Asaga and Ishigami, 2000, 2001), microglial cells (Asaga et al., 2002), and oligodendrocytes (Akiyama et al., 1999). However, we detected PAD2 earlier than GFAP, so PAD2 must be expressed in cells other than glial cells, possibly astrocytes. MAP2 and Nef3 were also expressed at an early embryonic stage in amounts that increased slightly until birth and remained almost constant until postnatal day 7 (Fig. 2A,D). Thus, PAD2 expression did not correlate with GFAP, MAP2, or Nef3 expression, indicating that PAD2 must appear at specific, but still unknown, stages and conditions of glial and neuronal cell differentiation.

In the cerebral cortex, cerebellum, and hippocampus, PAD2 mRNA expression increased significantly during the aging process (Fig. 4A). That is, PAD2 mRNA levels at the 30-month-old mark were 1.5-fold to 1.6-fold higher than in 3 month olds. Although GFAP mRNA expression also increased significantly during aging, the increase of GFAP did not correlate closely with that of PAD2, because GFAP in 30-month-old mice was 2.7-fold to 4.7-fold higher than that from 3 month olds, far exceeding the increase of PAD2. Moreover Nef3 mRNA expression did not change during aging. Because the change of PAD2 expression levels during aging did not correlate with those of GFAP and Nef3, PAD2 must be expressed only at certain times and under appropriate conditions by neuronal cells and glial cells, including astrocytes (Asaga and Ishigami, 2000, 2001), activated microglial cells (Asaga et al., 2002), and stage-specific immature oligodendrocytes (Akiyama et al., 1999).

Wood et al. (2008) reported that both PAD2 and PAD4 isoforms were present in myelin isolated from normal and MS white matter, and PAD4 was involved in histone citrullination in MS brain (Mastronardi et al., 2006). However, in this study, PAD4 protein was not detected at all by Western blot analysis with the PAD4-specific antibody we developed previously (Nakashima

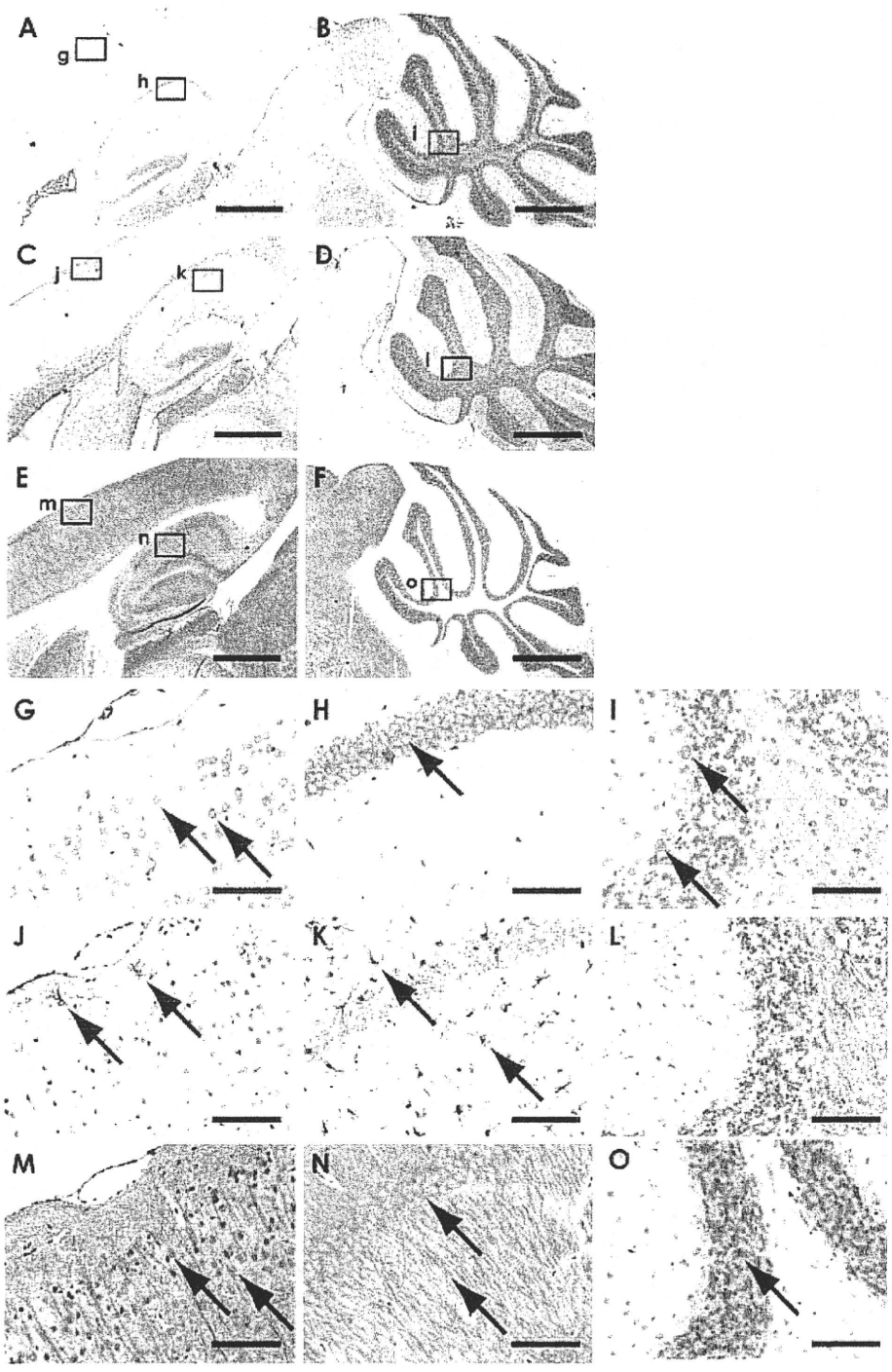

Fig. 5. Immunohistochemical staining of PAD2, GFAP, and MAP2 in the cerebral cortex, hippocampus, and cerebellum of 3-month-old mice. Each brain section was stained with PAD2 (**A,B,G–I**), GFAP (**C,D,J–L**), and MAP2 (**E,F,M–O**) antibody. The square area of g–i in A and B, j–l in C and D, and m–o in E and F were magnified for presentation in G–I, J–L, and M–O, respectively. Arrows indicate typical stained objects. Scale bars = 1 mm in A–F; 100 μm in G–O. [Color figure can be viewed in the online issue, which is available at www.interscience.wiley.com.]

et al., 1999). This discrepancy must be due to the different antibodies used. Moscarello et al. (1994) reported that approximately 20% of the total MBP was citrullinated in early developing human brain determined by protein sequencing; however, in this study, no citrullinated protein at all was found in the brain during normal development and aging by Western blot analysis with antimodified citrulline antibody (Senshu et al., 1992).

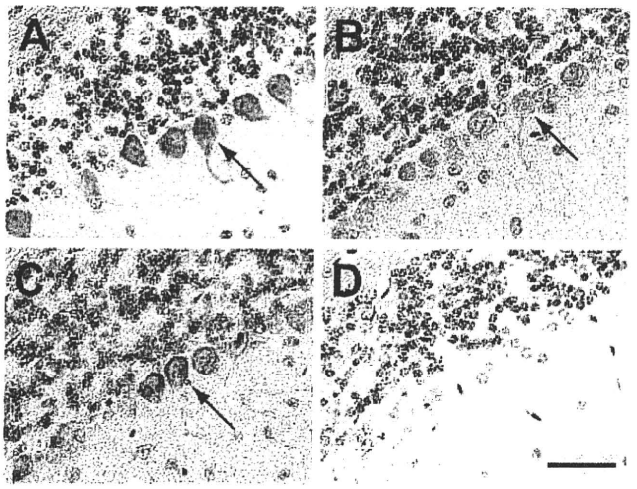

Fig. 6. Identification of PAD2-positive cells in the cerebellum by double immunostaining. Sections of cerebellum from 3-month-old mice were double immunostained with PAD2 and calbindin. Rabbit anticalbindin antibody was applied first, after which alkaline phosphatase-conjugated anti-rabbit IgG was applied for staining with the Red Alkaline Phosphate Substrate Kit I. Next, anti-PAD2 monoclonal antibody (hPAD2-2110) was applied; then, horseradish peroxidase-conjugated anti-mouse IgG was added to stain with DAB. The stained proteins are the following. **A:** Alkaline phosphate substrate as a chromogenic substrate (light magenta) for calbin. [Color figure can be viewed in the online issue, which is available at www.interscience.wiley.com.]

This discrepancy must be due to the technical differences between protein sequencing and Western blot analysis.

As described in our previous reports, PAD2 was detected in activated astrocytes in brains from AD and scrapie-infected mice (Ishigami et al., 2005; Jang et al., 2008). Many reports have, in fact, indicated that PAD2 normally remains inactive but becomes active and citrullinates cellular proteins only when the intracellular calcium balance is upset during neurodegenerative changes such as AD, prion disease, and MS (Moscarello et al., 1994; Ishigami et al., 2005; Jang et al., 2008). Thus, citrullinated protein has become a useful marker for neurodegenerative disorders of humans.

For the first time, PAD2 has been detected in Purkinje cells of the cerebellum, as we found by applying double-immunohistochemical staining for PAD2 and calbindin (Fig. 6). The cerebellum functions as the center of learning and control over motion, sensory input, and cognition. Purkinje cells of the cerebellum are its sole output neurons and are important as the integrators and fine tuners of diverse input signals (Cheron et al., 2008). Accumulated evidence indicates that the dynamic movement of Ca^{2+} plays a key role in the function of Purkinje cells (Matsushita et al., 2002; Erickson et al., 2007). Intracellular Ca^{2+} concentrations become elevated via voltage-dependent calcium channels of plasma membranes or inositol-1,4,5-triphosphate-dependent Ca^{2+} release from intracellular Ca^{2+} storage sites such as the endoplasmic reticulum (Cheron et al., 2008). Elevations of intracellular Ca^{2+} activate an intracellular signal cascade leading to such functional events as neurotransmitter release (Cheron et al., 2008). The relevance of this background is that the PAD enzyme requires ~100-fold higher than the normal intracellular Ca^{2+} level for its activation (Inagaki et al., 1989). Insofar as Purkinje cells store large amounts of Ca^{2+} corresponding to physiological stimuli (Matsushita et al., 2002), conceivably those intracellular Ca^{2+} concentrations become elevated transiently in specific, limited areas, such as near the endoplasmic reticulum and plasma membrane. When such a condition prevails, PAD2 enzyme would become activated and citrullinate various proteins, leading to cell death (Asaga et al., 1998). In fact, quantities of PAD2 and citrullinated proteins have been shown to increase in the brain in vivo during such abnormal conditions as scrapie-infection of mice and AD of humans (Ishigami et al., 2005; Jang et al., 2008).

In conclusion, we detected PAD2 mRNA in the brains of mice beginning at embryonic day 15 and tracked its ever-increasing expression in the cerebral cortex, hippocampus, and cerebellum until the animals were 30 months old. Moreover, we found here, for the first time, that PAD2 localized in neuronal cells of the cerebral cortex and Purkinje cells of the cerebellum. PAD2 may play a role in the onset and progression of neurodegenerative disorders by abnormally disrupting Ca^{2+} homeostasis and thereby increasing the production of citrullinated proteins.

ACKNOWLEDGMENT

We thank Ms. P. Minick for excellent editorial assistance.

REFERENCES

Akiyama K, Sakurai Y, Asou H, Senshu T. 1999. Localization of peptidylarginine deiminase type II in a stage-specific immature oligodendrocyte from rat cerebral hemisphere. Neurosci Lett 274:53–55.

Asaga H, Ishigami A. 2000. Protein deimination in the rat brain: generation of citrulline-containing proteins in cerebrum perfused with oxygen-deprived media. Biomed Res 21:197–205.

Asaga H, Ishigami A. 2001. Protein deimination in the rat brain after kainate administration: citrulline-containing proteins as a novel marker of neurodegeneration. Neurosci Lett 299:5–8.

Asaga H, Senshu T. 1993. Combined biochemical and immunocytochemical analyses of postmortem protein deimination in the rat spinal cord. Cell Biol Int 17:525–532.

Asaga H, Yamada M, Senshu T. 1998. Selective deimination of vimentin in calcium ionophore-induced apoptosis of mouse peritoneal macrophages. Biochem Biophys Res Commun 243:641–646.

Asaga H, Akiyama K, Ohsawa T, Ishigami A. 2002. Increased and type II-specific expression of peptidylarginine deiminase in activated microglia but not hyperplastic astrocytes following kainic acid-evoked neurodegeneration in the rat brain. Neurosci Lett 326:129–132.

Balcarek JM, Cowan NJ. 1985. Structure of the mouse glial fibrillary acidic protein gene: implications for the evolution of the intermediate filament multigene family. Nucleic Acids Res 13:5527–5543.

Cheron G, Servais L, Dan B. 2008. Cerebellar network plasticity: from genes to fast oscillation. Neuroscience 153:1–19.

Erickson MA, Haburcak M, Smukler L, Dunlap K. 2007. Altered functional expression of Purkinje cell calcium channels precedes motor dysfunction in tottering mice. Neuroscience 150:547–555.

Inagaki M, Takahara H, Nishi Y, Sugawara K, Sato C. 1989. Ca^{2+}-dependent deimination-induced disassembly of intermediate filaments involves specific modification of the amino-terminal head domain. J Biol Chem 264:18119–18127.

Ishigami A, Asaga H, Ohsawa T, Akiyama K, Maruyama N. 2001. Peptidylarginine deiminase type I, type II, type III and type IV are expressed in rat epidermis. Biomed Res 22:63–65.

Ishigami A, Ohsawa T, Asaga H, Akiyama K, Kuramoto M, Maruyama N. 2002. Human peptidylarginine deiminase type II: molecular cloning, gene organization, and expression in human skin. Arch Biochem Biophys 407:25–31.

Ishigami A, Ohsawa T, Hiratsuka M, Taguchi H, Kobayashi S, Saito Y, Murayama S, Asaga H, Toda T, Kimura N, Maruyama N. 2005. Abnormal accumulation of citrullinated proteins catalyzed by peptidylarginine deiminase in hippocampal extracts from patients with Alzheimer's disease. J Neurosci Res 80:120–128.

Jang B, Kim E, Choi JK, Jin JK, Kim JI, Ishigami A, Maruyama N, Carp RI, Kim YS, Choi EK. 2008. Accumulation of citrullinated proteins by up-regulated peptidylarginine deiminase 2 in brains of scrapie-infected mice: a possible role in pathogenesis. Am J Pathol 173:1129–1142.

Keilhoff G, Prell T, Langnaese K, Mawrin C, Simon M, Fansa H, Nicholas AP. 2008. Expression pattern of peptidylarginine deiminase in rat and human Schwann cells. Dev Neurobiol 68:101–114.

Laemmli UK. 1970. Cleavage of structural proteins during the assembly of the head of bacteriophage T4. Nature 227:680–685.

Lewis SA, Wang DH, Cowan NJ. 1988. Microtubule-associated protein MAP2 shares a microtubule binding motif with tau protein. Science 242:936–939.

Mastronardi FG, Wood DD, Mei J, Raijmakers R, Tseveleki V, Dosch HM, Probert L, Casaccia-Bonnefil P, Moscarello MA. 2006. Increased citrullination of histone H3 in multiple sclerosis brain and animal models of demyelination: a role for tumor necrosis factor-induced peptidylarginine deiminase 4 translocation. J Neurosci 26:11387–11396.

Matsushita K, Wakamori M, Rhyu IJ, Arii T, Oda S, Mori Y, Imoto K. 2002. Bidirectional alterations in cerebellar synaptic transmission of tottering and rolling Ca^{2+} channel mutant mice. J Neurosci 22:4388–4398.

Moscarello MA, Wood DD, Ackerley C, Boulias C. 1994. Myelin in multiple sclerosis is developmentally immature. J Clin Invest 94:146–154.

Moscarello MA, Mastronardi FG, Wood DD. 2007. The role of citrullinated proteins suggests a novel mechanism in the pathogenesis of multiple sclerosis. Neurochem Res 32:251–256.

Musse AA, Li Z, Ackerley CA, Bienzle D, Lei H, Poma R, Harauz G, Moscarello MA, Mastronardi FG. 2008. Peptidylarginine deiminase 2 (PAD2) overexpression in transgenic mice leads to myelin loss in the central nervous system. Dis Model Mech 1:229–240.

Nakashima K, Hagiwara T, Ishigami A, Nagata S, Asaga H, Kuramoto M, Senshu T, Yamada M. 1999. Molecular characterization of peptidylarginine deiminase in HL-60 cells induced by retinoic acid and 1α,25-dihydroxyvitamin D_3. J Biol Chem 274:27786–27792.

Senshu T, Sato T, Inoue T, Akiyama K, Asaga H. 1992. Detection of citrulline residues in deiminated proteins on polyvinylidene difluoride membrane. Anal Biochem 203:94–100.

Servais L, Bearzatto B, Schwaller B, Dumont M, De Saedeleer C, Dan B, Barski JJ, Schiffmann SN, Cheron G. 2005. Mono- and dual-frequency fast cerebellar oscillation in mice lacking parvalbumin and/or calbindin D-28k. Eur J Neurosci 22:861–870.

Tarcsa E, Marekov LN, Mei G, Melino G, Lee SC, Steinert PM. 1996. Protein unfolding by peptidylarginine deiminase. Substrate specificity and structural relationships of the natural substrates trichohyalin and filaggrin. J Biol Chem 271:30709–30716.

Towbin H, Staehelin T, Gordon J. 1979. Electrophoretic transfer of proteins from polyacrylamide gels to nitrocellulose sheets: procedure and some applications. Proc Natl Acad Sci U S A 76:4350–4354.

Tso JY, Sun XH, Kao TH, Reece KS, Wu R. 1985. Isolation and characterization of rat and human glyceraldehyde-3-phosphate dehydrogenase cDNAs: genomic complexity and molecular evolution of the gene. Nucleic Acids Res 13:2485–2502.

Vossenaar ER, Zendman AJ, van Venrooij WJ, Pruijn GJ. 2003. PAD, a growing family of citrullinating enzymes: genes, features and involvement in disease. Bioessays 25:1106–1118.

Watanabe K, Senshu T. 1989. Isolation and characterization of cDNA clones encoding rat skeletal muscle peptidylarginine deiminase. J Biol Chem 264:15255–15260.

Watanabe K, Akiyama K, Hikichi K, Ohtsuka R, Okuyama A, Senshu T. 1988. Combined biochemical and immunochemical comparison of peptidylarginine deiminases present in various tissues. Biochim Biophys Acta 966:375–383.

Whitney ER, Kemper TL, Bauman ML, Rosene DL, Blatt GJ. 2008. Cerebellar Purkinje cells are reduced in a subpopulation of autistic brains: a stereological experiment using calbindin-D28k. Cerebellum 7:406–416.

Wood DD, Ackerley CA, Brand B, Zhang L, Raijmakers R, Mastronardi FG, Moscarello MA. 2008. Myelin localization of peptidylarginine deiminases 2 and 4: comparison of PAD2 and PAD4 activities. Lab Invest 88:354–364.

Acta Neuropathol
DOI 10.1007/s00401-009-0625-x

ORIGINAL PAPER

Involvement of peptidylarginine deiminase-mediated post-translational citrullination in pathogenesis of sporadic Creutzfeldt-Jakob disease

Byungki Jang · Jae-Kwang Jin · Yong-Chul Jeon · Han Jeong Cho · Akihito Ishigami · Kyung-Chan Choi · Richard I. Carp · Naoki Maruyama · Yong-Sun Kim · Eun-Kyoung Choi

Received: 23 July 2009 / Revised: 27 November 2009 / Accepted: 5 December 2009

Abstract Peptidylarginine deiminases (PADs)-mediated post-translational citrullination processes play key roles in protein functions and structural stability through the conversion of arginine to citrulline in the presence of excessive calcium concentrations. In brain, PAD2 is abundantly expressed and can be involved in citrullination in disease. Recently, we have reported pathological characterization of PAD2 and citrullinated proteins in scrapie-infected mice, but the implication of protein citrullination in the pathophysiology in human prion disease is not clear. In the present study, we explored the molecular and biological involvement of PAD2 and the pathogenesis of citrullinated proteins in frontal cortex of patients with sporadic Creutzfeldt-Jakob disease (sCJD). We found increased expression of PAD2 in reactive astrocytes that also contained increased levels of citrullinated proteins. In addition, PAD activity was significantly elevated in patients with sCJD compared to controls. From two-dimensional gel electrophoresis and MALDI-TOF mass analysis, we found various citrullinated candidates, including cytoskeletal and energy metabolism-associated proteins such as vimentin, glial fibrillary acidic protein, enolase, and phosphoglycerate kinase. Based on these findings, our investigations suggest that PAD2 activation and aberrant citrullinated proteins could play a role in pathogenesis and have value as a marker for the postmortem classification of neurodegenerative diseases.

Keywords Citrullination · Peptidylarginine deiminase · Creutzfeldt-Jakob disease · Prion · Astrocytes

Abbreviations

PAD	Peptidylarginine deiminase
CJD	Creutzfeldt-Jakob disease
PrP	Prion protein
CNS	Central nervous system
2-DE	Two-dimensional gel electrophoresis
MALDI-TOF mass	Matrix-assisted laser desorption/ ionization-time of flight mass
BAEE	Benzoyl-L-arginine ethyl ester
SDS	Sodium dodecyl sulfate
anti-MC	Anti-modified citrulline
GAPDH	Glyceraldehyde-3-phosphate dehydrogenase

B. Jang · J.-K. Jin · Y.-C. Jeon · H. J. Cho · Y.-S. Kim · E.-K. Choi
Ilsong Institute of Life Science, Hallym University, Anyang, Republic of Korea

B. Jang · Y.-S. Kim
Department of Microbiology, College of Medicine, Hallym University, Chuncheon, Republic of Korea

A. Ishigami
Department of Biochemistry, Faculty of Pharmaceutical Sciences, Toho University, Chiba, Japan

A. Ishigami · N. Maruyama
Tokyo Metropolitan Institute of Gerontology, Itabashi-ku, Tokyo, Japan

K.-C. Choi
Department of Pathology, College of Medicine, Hallym University, Chuncheon, Republic of Korea

R. I. Carp
New York State Institute for Basic Research in Developmental Disabilities, Staten Island, New York, USA

E.-K. Choi (✉)
Laboratory of Cellular Aging and Neurodegeneration, Ilsong Institute of Life Science, Hallym University, Anyang, Gyeonggi-do 431-060, Republic of Korea
e-mail: ekchoi@hallym.ac.kr

Published online: 16 December 2009

GFAP	Glial fibrillary acidic protein
MBP	Myelin basic protein
AD	Alzheimer's disease

Introduction

Prion diseases are a group of progressive neurodegenerative diseases that affect the central nervous system (CNS) in humans and animals. These are rare, infectious, and fatal neurodegenerative diseases that are characterized by spongiform changes, neuronal degeneration, reactive gliosis, and accumulation of disease-associated misfolded prion proteins (termed PrP^{Sc}) in the CNS [51]. In prion diseases, PrP^{Sc} is a factor in causation and is thought of as an unconventional infectious agent. Sporadic Creutzfeldt-Jakob disease (sCJD) is the most common of the human diseases, accounting for approximately 85% of human prion cases; it occurs at a rate of approximately one per million [34]. The etiological factor of sCJD remains unknown; in contrast, variant CJD is transmitted from bovine spongiform encephalopathy, and familial CJD (fCJD) is caused by a point mutation at a codon of the prion protein [1, 51].

The post-translational modifications of various proteins are important events required in the regulation of many cellular processes. Aberrant and excessive modifications can provoke abnormal conditions; in particular, these modifications have emerged as key events of CJD development and pathogenesis. These modifications include glycosylation, nitration, phosphorylation, and lipoxidation [17, 20, 45, 46]. Among various post-translational modifications, citrullination (or deimination) is an irreversible process that converts protein-bound arginine residues to citrulline which results in loss of their positive charge, provokes a conformational change, and alters the isoelectric point (*p*I) value and electrophoretic-mobility [58]. Peptidylarginine deiminases (PADs) regulate this process by their activation along with up-regulation of intracellular calcium (Ca^{2+}) distribution [60]. PADs are found as five different isoforms (types 1–4, and 6) that are distinct in substrate and tissue specificity [60]. Among them PAD2 and PAD4 are localized in the CNS [24, 25, 36, 40, 60, 62] and PAD2 is also ubiquitously distributed in other mammalian tissues such as muscle, dermis, spleen, and hematopoietic cells [37, 60]. Especially PAD2 is abundantly expressed in brain which citrullinates various cytoplasmic proteins such as glial fibrillary acidic protein (GFAP) and myelin basic protein (MBP) [24, 38]. PAD2 has been reported to contribute to pathogenic events in abnormal conditions [5, 7, 24, 25, 32, 38], and is abundantly increased in reactive astrocytes during several neurodegenerative conditions [24, 25, 43]. Distinctively, PAD4 is the only type of PAD that has a nuclear localization signal sequence at N-terminal domain [2], resulting in localization in cell nuclei where the enzyme citrullinates histones [36, 41, 61]. Since the five Ca^{2+}-binding sites were found in PAD4 by structural analysis [2] and were conserved with several other isoforms [37], it is presumed that PAD2 also contains five Ca^{2+}-binding sites. Under abnormal conditions, PADs-mediated citrullinations have been shown to affect various biological functions, such as the change of proteolytic susceptibility, binding affinity to target molecules, inflammatory processes induced by autoantibodies, regulation of gene expression, and cellular structural changes [31, 35, 49, 50, 61].

Increased citrullination and/or upregulated PAD have been reported in a number of human diseases including multiple sclerosis [36, 38, 43], rheumatoid arthritis [23, 32], Alzheimer's disease (AD) [24], cancer [10, 11], dermatosis [37, 60], and an experimental mouse model of prion disease [25]. The occurrence of citrullinated proteins is associated with disease development or progression, and it could serve as a useful marker or therapeutic target for human diseases.

Recently, we reported pathological characterization of PAD2 and citrullinated proteins that were abnormally accumulated in various brain regions of ME7 scrapie-infected mice [25]. For human prion diseases, the role of citrullination remains to be assessed. In the present study, we explored the molecular and biological involvement of PAD2 and citrullinated proteins in frontal cortex of patients with sCJD.

Materials and methods

Patients

Human brain tissues were obtained from the Biosafety Level-III Autopsy Center for CJD (Hallym University Sacred Heart Hospital, Republic of Korea). The sliced brain tissues were stored at −80°C until analysis. The study was approved by the Institutional Review Board at Hallym University. The pathologic features of the CJD patients are summarized in Table 1 and Fig. 1.

Western blot analysis

Brain tissues were homogenized in 50 mM Tris–HCl, pH 7.4, 150 mM NaCl, 1 mM EDTA, 1 mM sodium vanadate, 1% Triton X-100, 1% Nonidet P-40, 0.25% sodium deoxycholic acid, and protease inhibitors (Roche diagnostics, Indianapolis, IN, USA). For detection of PrP^{Sc}, samples were digested with 20 μg/ml proteinase-K (PK)

Table 1 Clinical details of controls and CJD patients specimens

No.	Diagnosis	Sex	Age	Brain weight (g)	Postmortem interval (h)
1	Non-CJD	M	83	1,220	12.0
2	Non-CJD	F	67	1,400	4.0
3	Non-CJD	M	71	1,225	7.0
4	Non-CJD	M	55	1,280	12.0
CJD1	Sporadic	M	77	1,600	2.5
CJD2	Sporadic	M	49	1,150	120.0
CJD3	Sporadic	F	66	1,380	13.0
CJD4	Familial	F	66	1,450	13.5

All non-CJD cases are normal brains. Familial CJD has a point mutation of valine to isoleucine at codon 203 of the prion protein

for 40 min at 37°C and then were probed with mouse monoclonal anti-PrP (3F4, 1:500) [29]. For detection of citrullinated proteins, 50 μg of protein was subjected to 12% SDS–PAGE, transferred to PVDF membrane followed by incubation in modification reagent [1 v of a mixture of 1% diacetyl monoxime/0.5% antipyrine/1 M acetic acid, and 2 v of a mixture of 85% H_3PO_4/98% H_2SO_4/H_2O (20/25/55) containing 0.1% $FeCl_3 \cdot 6H_2O$] and probed with a rabbit polyclonal anti-modified citrulline antibody (anti-MC) at 1:1,000 (Upstate, Lake Placid, NY, USA) as described previously [54]. For the detection of other target proteins, the transferred PVDF membranes were directly probed with mouse monoclonal anti-PAD2 (1:5,000) [56], rabbit polyclonal anti-GFAP (1:7,000, Dr. Ishigami generation) or rabbit polyclonal anti-GAPDH (1:1,000) (Santa Cruz Biotechnology, Santa Cruz, CA, USA). The membranes were then incubated with the appropriate secondary antibody-conjugated HRP. Bound antibodies were visualized by chemiluminescent substrate as described by the manufacturer (Amersham Biosciences, Piscataway, NJ, USA).

Immunohistochemistry

Neutral buffered formalin-fixed brains were cut into 6-μm thick slices and the sections were used for immunohistochemical staining. For staining of citrullinated proteins, the experiment was performed as described previously [25]. For negative control of staining of citrullinated proteins, the sections were incubated with dH_2O instead of 1 v of a mixture of 1% diacetyl monoxamine, 0.5% antipyrine, and 1 N acetic acid. After incubation with primary antibodies including mouse monoclonal anti-PrP (3F4, 1:200), rabbit polyclonal anti-GFAP (1:500, Dako, Copenhagen, Denmark), mouse monoclonal anti-PAD2 (2110, 1:100), and rabbit polyclonal anti-MC (1:400), the sections were washed and then treated sequentially with biotinylated anti-mouse IgG or anti-rabbit IgG, and then incubated with avidin–biotin peroxidase complex using the ABC kit (Vector, Burlingame, CA, USA), developed with 0.003% 3,3-diaminobenzidine and 0.03% H_2O_2 in 50 mM Tris buffer, and finally hematoxylin-counterstained sections were examined under light microscope (BX51; Olympus, UK). For immunofluorescence staining, primary antibodies-exposed sections were labeled with LRSC-conjugated donkey anti-rabbit IgG (1:200) or FITC-conjugated goat anti-mouse IgG (1:200) (Jackson ImmunoResearch, West Grove, PA, USA),

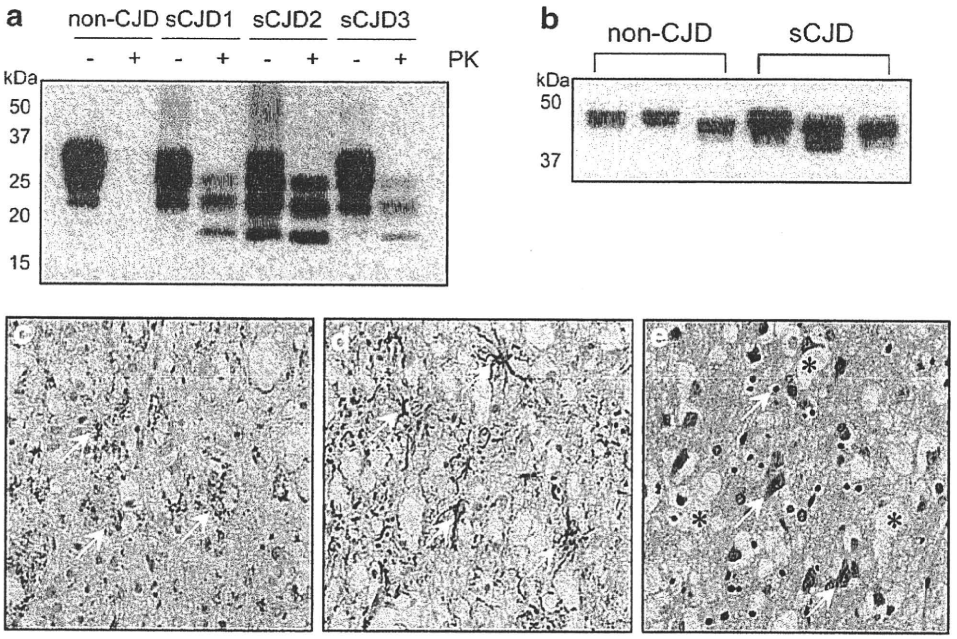

Fig. 1 Pathological characterization of brain samples from sCJD patients. **a** Proteinase K-(PK)-resistant PrP^{Sc} analysis by Western blotting using anti-PrP antibody. **b** Western blot analysis of GFAP expression using anti-GFAP antibody. **c–e** Histological characterizations including PrP^{Sc} deposition in the PK-treated brain slice (**c**), cell bodies and processes of reactive astrocytes (**d**), and vacuolation by hematoxylin–eosin staining (**e**) in frontal cortex of sCJD patients. *Arrows* indicate PrP^{Sc} (**c**), GFAP-positive astrocytes (**d**), and cell body and nucleus of neuronal cell or glial cell in the section. *Asterisks* indicate vacuoles as distinct holes. Original magnification ×20